Article:
Antoniadou, I., Manson, G., Staszewski, W.J. et al. (2 more authors) (2015) A time-frequency analysis approach for condition monitoring of a wind turbine gearbox under varying load conditions. Mechanical Systems and Signal Processing, 64-65. 188 - 216. ISSN 0888-3270

https://doi.org/10.1016/j.ymssp.2015.03.003

A time-frequency analysis approach for condition monitoring of a wind turbine gearbox under varying load conditions

I. Antoniadou[a], G. Manson[a], W. J. Staszewski[b], T. Barszcz[b], K. Worden[a]

[a] *Dynamics Research Group, Mechanical Engineering Department, The University of Sheffield, Mappin Street, Sheffield S1 3JD, United Kingdom*
[b] *Department of Robotics and Mechatronics, Faculty of Mechanical Engineering and Robotics, AGH University of Science and Technology, Al. Mickiewicza 30, 30-059 Krakow, Poland*

Abstract

This paper deals with the condition monitoring of wind turbine gearboxes under varying operating conditions. Generally, gearbox systems include nonlinearities so a simplified nonlinear gear model is developed, on which the time-frequency analysis method proposed is first applied for the easiest understanding of the challenges faced. The effect of varying loads is examined in the simulations and later on in real wind turbine gearbox experimental data. The Empirical Mode Decomposition (EMD) method is used to decompose the vibration signals into meaningful signal components associated with specific frequency bands of the signal. The mode mixing problem of the EMD is examined in the simulation part and the results in that part of the paper suggest that further research might be of interest in condition monitoring terms. For the amplitude-frequency demodulation of the signal components produced, the Hilbert Transform (HT) is used as a standard method. In addition, the Teager-Kaiser energy operator (TKEO), combined with an energy separation algorithm, is a recent alternative method, the performance of which is tested in the paper too. The results show that the TKEO approach is a promising alternative to the HT, since it can improve the estimation of the instantaneous spectral characteristics of the vibration data under certain conditions.

Keywords: condition monitoring, wind turbine gearboxes, time-varying loads, empirical mode decomposition, Teager-Kaiser energy operator, Hilbert Transform.

Email address: I.Antoniadou@shef.ac.uk; (I. Antoniadou)

1. Introduction

Statistics show that the most frequent damages observed in wind turbine systems are in the electrical control components, the blades, the main bearing and the gearboxes and that the most responsible component for downtime is the gearbox [1]. This means that condition monitoring of wind turbine gearboxes is a necessary practice. Vibration analysis is a commonly used approach for condition monitoring, and is based on the idea that the rotating machinery have a specific vibration signature for their standard condition that changes with the development of damage. Vibration based condition monitoring should be a relatively easy task for gearboxes operating under steady conditions, as offered in laboratory environments. Unfortunately, working wind turbine gearboxes have a vibration signature that is also affected by the environmental conditions (temperature variations, wind turbulence) and time varying loads under which they operate. The load variations of wind turbine gearboxes are far from smooth and are usually nondeterministic, and since vibration signals tend to change with speed and load of the gearbox, varying loads (and/or speeds) might not necessarily generate stationary signals. In this case, false alarms could be created in the signals and damage features might be influenced by the variations. This makes condition monitoring of wind turbine gearboxes a difficult matter, since the signal processing that is required in this case should overcome the problem of nonstationary influences in the signals not related to damage.

In general, condition monitoring methods do not differ from other damage detection methods apart from the fact that one knows *a priori* about the frequency bands related to damage, for the gears, bearings and other components. A review of methods used for damage detection is given in Ref. [2]. In the early studies, some of the conventional techniques used for condition monitoring were the probability distribution characteristics of the vibration such as the skewness and kurtosis [3], the Fourier spectrum and modulation sidebands [4, 5] and Cepstrum analysis [6]. These methods have been widely used for condition monitoring and were proved to work well under certain conditions, such as steady loading of the gearboxes. Unfortunately, in the majority of cases, gearbox signals have spectral characteristics that vary with time. This variation with time cannot be obtained using the Fourier transform as this transform simply expands a signal as a linear combination of single frequencies that exist over all time. This drawback was the motivation for greater attention to time-frequency analysis methods such as the Wigner-Ville distribution [7], wavelet analysis [8] and cyclostationary analysis [9]. Wavelet analysis is probably the most popular technique [10], but has the drawback that the basis functions of the decompositions are fixed and do not necessarily match the varying nature of the signals. Relatively recently, the Empirical Mode Decomposition (EMD) method was also proposed [11]. Since then, attention was placed on applying the EMD

in the damage detection field [12, 13]. This technique decomposes the signal into a number of meaningful signal components, representing simple oscillatory modes matched to the specific data. This is one of the basic advantages of the EMD when compared to other time-frequency methods. After decomposing the vibration signal, the instantaneous frequency and amplitude of each component can be estimated, most commonly by applying the Hilbert Transform (HT). An alternative approach in order to obtain the instantaneous characteristics of the decomposed vibration signals, is to use an energy tracking operator to estimate the energy of the signal, as developed by Teager [14, 15] but first introduced by Kaiser [16, 17], and then use an energy separation algorithm for the estimation of the amplitude envelope and instantaneous frequency of each signal component produced by the EMD method. This method promises high resolution and low computational power. That is why some primary studies occurred in the literature [18, 19, 20] associated with the application of this energy operator in machinery fault diagnosis. Ref. [20] focuses on the application of this operator to the fault diagnosis of wind turbine planetary gearboxes, where the challenge was the planetary gearbox signals‘ spectral complexity under steady load conditions. What the current study aims for is to show how the challenges of load variations of wind turbine gearbox vibration signals can be overcome using a time-frequency approach, in this case the EMD method in combination with the TKEO and an energy separation algorithm. The experimental datasets used in this paper are obtained from a real wind turbine gearbox in operation, as opposed to many other studies. In addition, only few previous studies go beyond the application of new time-frequency methods in condition monitoring and examine the effects of time varying loads in the gearbox vibration signals when trying to do condition monitoring [21, 22, 23, 24]. In these references the use of the signal RMS value, or the arithmetic sum of the amplitudes of the spectral gearmesh components as well as the use of the short-time Fourier transform and the Wigner-Ville distribution are applied.

It is difficult to state all the advantages and disadvantages of the EMD method and other filter bank methods, such as the short time Fourier Transform (STFT) or the wavelets mainly because of their different theoretical background. It is also reasonable to claim that for different situations different methods might work better than the others. The wavelet transform and the STFT are similar in a mathematical sense, both methods decompose the signal to be analysed by convolving it with a predefined “basis”, e.g. the mother wavelet for the case of the wavelet transform. It might be easier to compare these two methods in that sense, although this is beyond the purpose of the current paper, since it is the EMD method that the authors are currently examining. Considering the case of the wavelet transform the choice of mother wavelets might influence the results of the analysis. Also assumption of stationarity during a time-span of the mother wavelet (or

window for the STFT) might inhibit the estimation of the subtle changes in the frequencies. On the contrary, the EMD method is not exactly equivalent on its own to the previously mentioned methods. The procedure of the decomposition, not mathematically proven yet, is based on the adaptation to the geometric characteristics of the signal, without leaving the time-domain. The method decomposes the signal by using information related to the local characteristics for each time-scale of the signal. Being an adaptive method, it represents better the mechanisms hidden in the data, no pre-defined basis function or mother wavelet is needed during the process since the decomposition is completely data-driven. The adaptivity is therefore one major advantage of the method and also in some cases its ability to better estimate subtle changes in the signal, due to the fact that one doesn't use any kind of window function in the process and doesn't need to assume stationarity for any time-span of the signal. As for the case of every method of course, the EMD has some limitations too. The most known ones are the end effect and the mode mixing problems that will be described in more detail in the next sections of the paper.

The structure of the paper is going to be the following: in Section 2 the gear model used in the simulation part of the work will be thoroughly described, as well as the type of loads and the kind of fault introduced to the model. The purpose of the simulation is basically to test how the time frequency analysis method proposed corresponds to the simulated signals in order to have an initial idea of the kind of damage features one should expect in the real wind turbine data. In addition, the effect of load variation in the signals will be examined in this simulation environment, which is more controlled and easier to understand. In Section 3 the experimental datasets from the wind turbine gearbox vibration data will be presented. The two signal processing methods, the standard Hilbert-Huang Transform, and the alternative approach proposed in the current paper, consisting of combining the EMD, the TKEO and an energy separation algorithm, will be explained in detail in Section 4. Finally, the results for both the simulation and the experimental data will be discussed in Section 5. Conclusions will be given in Section 6.

2. Gearbox simulation

2.1. Theoretical model

Many scientific teams have examined the subject of dynamic gear behaviour and various mathematical gear models have been developed in the past. These models can be categorised into linear time-varying and nonlinear time-varying. Linear gear models are arguably too simplified, and for the sake of accuracy nonlinear models should be used. This is because the geometrical characteristics of the gear teeth affect the dynamics of the gear systems. The varying gear tooth contact ratio causes a variation of the gear

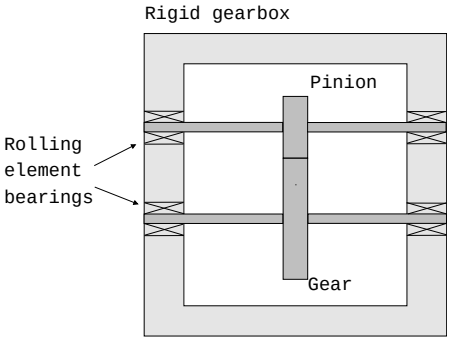

(a) A generic geared rotor bearing system.

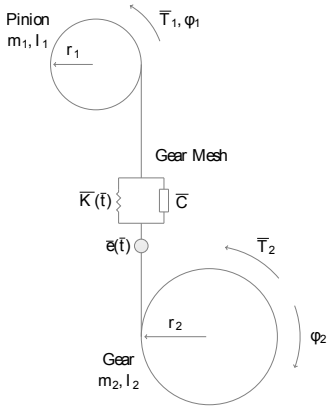

(b) 2DOF nonlinear gear model.

meshing stiffness. Gear backlash, which is introduced either intentionally at the design stages or caused by wear makes the equations of motion of gear systems nonlinear. This is the reason why many of the analytical gear models developed served in the study of nonlinearities in gears, parametric friction instabilities, nonlinear frequency response of gears and bifurcation [25, 26, 27, 28, 29, 30, 31, 32]. Reviews of gear dynamic models are given in the references [33, 34, 35].

A generic geared-rotor bearing system consisting of a spur gear pair mounted on flexible shafts, supported by rolling element bearings [27], is shown in Fig. 1a. The governing equations of motion can be given in matrix form as:

$$[\overline{M}]\{\ddot{\overline{q}}(\bar{t})\} + [\overline{C}]\{\dot{\overline{q}}(\bar{t})\} + [\overline{K}(\bar{t})]\{f(\overline{q}(\bar{t}))\} = \{\overline{F}(\bar{t})\} \tag{1}$$

where $[\overline{M}]$ is the time-invariant mass matrix, $\{\overline{q}(\bar{t})\}$ is the displacement vector, $[\overline{C}]$ is the damping matrix (assumed to be time-invariant), $[\overline{K}(\bar{t})]$ is the stiffness matrix considered to be periodically time-varying, $\{f(\overline{q}(\bar{t}))\}$ is a nonlinear displacement vector that includes the radial clearances in bearings and gear backlash and $\{\overline{F}(\bar{t})\}$ the external torque and internal static transmission error excitations.

2.2. Dimensional model

The system of Fig. 1a can be described by the two-degree-of-freedom nonlinear model shown in Fig. 1b, which has been used in previous studies [27, 29]. Its validity has also been compared with experimental results [27]. The gear mesh is described by a nonlinear displacement function $B(\overline{x}(\bar{t}))$ with time-varying stiffness $\overline{K}(\bar{t})$ and linear viscous damping $\overline{C}$. The bearings and shafts that support the gears are assumed to be rigid. The input torque fluctuation is included but the output torque is considered to be constant: $\overline{T}_1(\bar{t}) = T_{te}(\bar{t}) + \overline{T}_{1var}(\bar{t})$ and $\overline{T}_2(\bar{t}) = \overline{T}_{2m}$, with $\overline{T}_{2m}$ being the mean output torque, $T_{te}(\bar{t})$ is related to transmission error excitations and $\overline{T}_{1var}(\bar{t})$ the

external input torque fluctuation. In this simulation $\overline{T}_1(\bar{t})$ includes a torque produced using the FAST design code [36], and will be discussed in detail in a following section. The main purpose of introducing this input to the model is to add loads similar to those that wind turbine gearboxes experience; previous models of gears have not included such a characteristic.

The equations of motion describing the gear model given in the general form are the following, where $\phi_i(\bar{t})$ is the torsional displacement, r_i is the base radius, and I_i is the mass moment of inertia of the i_{th} gear:

$$I_1\ddot{\phi_1}(\bar{t}) + r_1\overline{C}\dot{\overline{x}}(\bar{t}) + r_1 B(\overline{x}(\bar{t}))\overline{K}(\bar{t}) = \overline{T}_1(\bar{t}) \tag{2}$$

$$I_2\ddot{\phi_2}(\bar{t}) - r_2\overline{C}\dot{\overline{x}}(\bar{t}) - r_2 B(\overline{x}(\bar{t}))\overline{K}(\bar{t}) = -\overline{T}_2(\bar{t}) \tag{3}$$

The gear meshing frequency is given by:

$$\overline{\Omega}_{mesh} = n_1\overline{\Omega}_1 = n_2\overline{\Omega}_2 \tag{4}$$

where n_1 and n_2 stand for the number of teeth of each gear and $\overline{\Omega}_i$ is the rotating frequency of the i_{th} gear.

The meshing stiffness and the static transmission error are assumed to be periodic functions of time and can be expressed in a Fourier series form:

$$\overline{K}(\bar{t}) = \overline{K}(\bar{t} + \frac{2\pi}{\overline{\Omega}_{mesh}}) = \overline{K}_m + \sum_{j=1}^{\infty} \overline{K}_j cos(j\overline{\Omega}_{mesh}\bar{t} + \phi_{kj}) \tag{5}$$

$$\overline{e}(\bar{t}) = \overline{e}(\bar{t} + \frac{2\pi}{\overline{\Omega}_{mesh}}) = \sum_{j=1}^{\infty} \overline{e}_j cos(j\overline{\Omega}_{mesh}\bar{t} + \phi_{ej}) \tag{6}$$

In the above equations $\overline{K}_m$, $\overline{K}_j$ and $\overline{e}_j$ are the constant Fourier coefficients.

The transmission error is the difference between the actual position of the output gear and the position it would occupy if the gear drive were manufactured perfectly. The transmission error in two meshing gears consists mainly of pitch error, profile error and run-out error.

The mesh stiffness on the other hand varies due to the transition from single to double and from double to single pairs of teeth in contact.

The nonlinear displacement function related to the gear backlash nonlinearity is given by:

$$B(\overline{x}(\bar{t})) = \begin{cases} \overline{x}(\bar{t}) - b_g, & \overline{x}(\bar{t}) \geq b_g \\ 0, & -b_g < \overline{x}(\bar{t}) < b_g \\ \overline{x}(\bar{t}) + b_g, & \overline{x}(\bar{t}) \leq -b_g \end{cases} \tag{7}$$

where $2b_g$ represents the total gear backlash. The gear tooth backlash function controls the contact between teeth and allows for the fact that occasionally contact is lost.

The difference between the dynamic transmission error and the static transmission error is described as:

$$\overline{x}(\bar{t}) = r_1\phi_1(\bar{t}) - r_2\phi_2(\bar{t}) - \overline{e}(\bar{t}) \tag{8}$$

The equation (8) helps in describing the original model with a single equation of motion:

$$m_c\ddot{\overline{x}}(\bar{t}) + \overline{C}\dot{\overline{x}}(\bar{t}) + \overline{K}(\bar{t})B(\overline{x}(\bar{t})) = \overline{F}_m + \overline{F}_{te}(\bar{t}) + \overline{F}_{var}(\bar{t}) \tag{9}$$

where:

$$m_c = \frac{I_1 I_2}{I_1 r_2^2 + I_2 r_1^2} \tag{10}$$

$$\overline{F}_m = \frac{\overline{T}_{1m}}{r_1} = \frac{\overline{T}_{2m}}{r_2} \tag{11}$$

$$\overline{F}_{te}(\bar{t}) = -m_c\ddot{\overline{e}}(\bar{t}) \tag{12}$$

Now concerning the equations related to the FAST loads input in the model: $\overline{F}_{var}(\bar{t}) = \frac{r_1 I_2 \overline{T}_{1var}(\bar{t}) - r_2 I_1 \overline{T}_2(\bar{t})}{I_1 r_2^2 + I_2 r_1^2}$, $\overline{T}_{1var}(\bar{t}) = \overline{T}_{FAST} - \overline{T}_{FASTmean}$, $\overline{T}_{1m} = \overline{T}_{FASTmean}$. A specific section later on discusses these loads.

2.3. Dimensionless model

The equations of motion of the model can be written in a dimensionless form by letting: $x(\bar{t}) = \frac{\overline{x}(\bar{t})}{b_g}$, $w_n = \sqrt{\frac{\overline{K}_m}{m_c}}$, $z = \frac{\overline{C}}{2\sqrt{m_c \overline{K}_m}}$, $K(\bar{t}) = \frac{\overline{K}(\bar{t})}{\overline{K}_m}$, $F_{te}(\bar{t}) = \frac{\overline{F}_{te}(\bar{t})}{m_c b_g w_n^2} = \frac{-m_c\ddot{\overline{e}}(\bar{t})}{m_c b_g w_n^2}$, $F_{var}(\bar{t}) = \frac{\overline{F}_{var}(\bar{t})}{m_c b_g w_n^2}$ and $t = w_n\bar{t}$. Furthermore, the nondimensional excitation frequency is: $\Omega_{mesh} = \frac{\overline{\Omega}_{mesh}}{w_n}$. Fig. 2a shows the diagram of the gear meshing stiffness (nondimensional values) and Fig. 2b the diagram of the static transmission error, (STE), used in the gear model simulations.

The nondimensional form of the original equation of motion is:

$$\ddot{x}(t) + 2z\dot{x}(t) + K(t)B(x(t)) = F_m + F_{te}(t) + Fvar(t) \tag{13}$$

where the backlash function can be expressed as:

$$B(x(t)) = \begin{cases} x(t) - 1, & x(t) \geq 1 \\ 0, & -1 < x(t) < 1 \\ x(t) + 1, & x(t) \leq -1 \end{cases} \tag{14}$$

Fig. 3 shows the form of backlash function.

The model was encoded in MATLAB functions and was solved with the *ode45* differential equation solver, with a fixed step of 0.015. The parameters used for the simulation are chosen according to Ref. [27] and are described in Table 1.

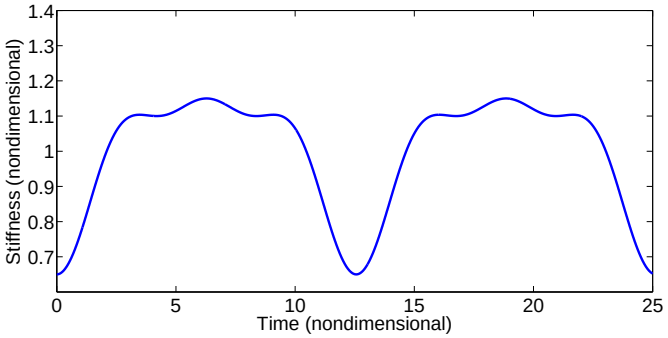

(a) The gear meshing stiffness function.

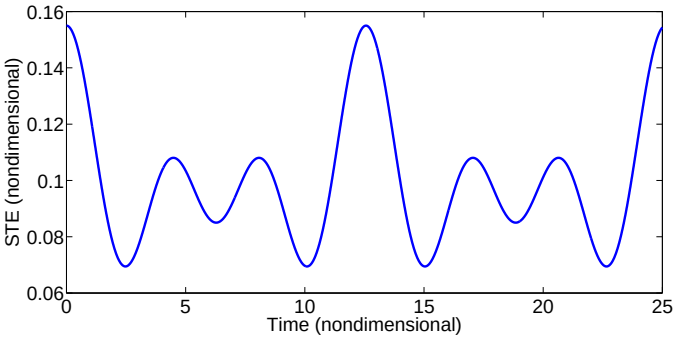

(b) The STE function.

In the simulations presented in the paper for the case where no varying load is applied to the model, single-sided tooth impact was observed (tooth separation without back collision, backlash region $-1 < x(t) < 1$) for 20.6% of the simulation samples. For the case where the simulated varying load was applied, single-sided tooth separation was observed again for 23.5% of the simulation samples. In neither case was double-sided impact observed (backlash region $x(t) < -1$). The time varying meshing stiffness, due to the Fourier series form expression chosen to describe it and the non-dimensional values given in Table 1 ($k_1 = 0.2$, $k_2 = 0.1$ and $k_3 = 0.05$), has a $\pm 35\%$ variation around the mean. Due to the stiffness variations, the natural frequency varies also, in the range $0.8 < w_n < 1.16, (w_n = \sqrt{\frac{\overline{K}_m}{m_c}})$. The dimensionless meshing frequency is given in Table 1 and is 0.5; so a 0.015 (dimensionless) time step corresponds to a sampling frequency of 67 (dimensionless) and is certainly large enough to prevent aliasing.

Changing certain values according to the Ref. [27] could help in order to have stronger nonlinear behaviour, but that was not the primary concern of the study.

Despite the fact that this is a very simple wind turbine gearbox model, since it consists of only one spur gear stage and it ignores the bearing vibrations, when in reality wind turbine gearboxes usually consist of three gear

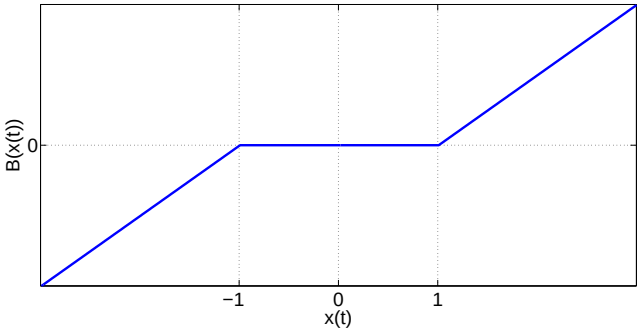

Figure 3: The backlash function.

Table 1: Simulation parameters

$I_{1,2} = 0.00115\ [kg\ m^2]$
$m_c = 0.23\ [kg]$
$r_{1,2} = 0.094\ [m]$
$number\ of\ teeth = 16$
$\overline{K}_m = 3.8 \cdot 10^8\ [\frac{N}{m}]$
$b_g = 0.1 \times 10^{-3}\ [m]$
$z = 0.05$
$\Omega_{mesh} = 0.5$
$F_m = 0.1$
$F_{te1} = 0.01$
$F_{te2} = 0.04$
$F_{te3} = 0.02$
$k_1 = 0.2$
$k_2 = 0.1$
$k_3 = 0.05$

stages with one or two being planetary stages and the rest, parallel spur gear stages, it is sufficient for the current study. The reason is that the time frequency method that will be used further on has the ability to isolate specific frequency components of the signal. More gear stages in a vibration signal would mean more frequency components at different frequency bands. Damage at a specific gear stage would therefore be "shown" in the vibration signal associated with the meshing frequency and its harmonics of the gear stage examined. What is important in this gear model, and the main purpose of the simulations, is to show how time varying loads, similar to those observed in wind turbines, influence the vibration signals, and how the time-frequency analysis methods proposed help in this case to overcome the challenges produced by these influences.

2.4. Gear tooth faults

Certain types of gear tooth damage cause a reduction in gear tooth stiffness. These types of damage can be modelled here by reducing the stiffness function periodically, with the period of the rotation of the gear with the damaged tooth. Tooth stiffness is a key parameter in gear dynamics concerning the determination of factors such as dynamic tooth loads and the vibration characteristics of the geared system. The changes due to the tooth damage appear in the vibration spectrum as amplitude and phase modulations [37, 38, 39, 40]. This has an effect on the acceleration waveform as well, to be more specific a local increase of the acceleration magnitude can be observed. Briefly, the mechanism is the following: when the defected tooth accepts the load, the crack opens gradually with the increase of load up to the point where the load reaches its maximum level. Then, the load is gradually transferred to nearby teeth and the crack steadily closes. This occurs once per shaft revolution.

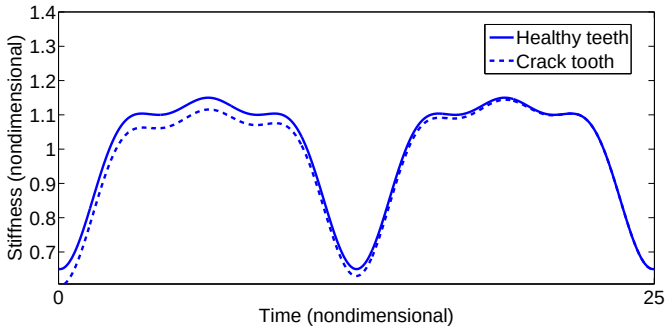

Figure 4: The meshing stiffness for healthy teeth and for a tooth with crack (0.3% stiffness reduction).

Concerning the simulation here, a gear fault was introduced into the model by reducing the meshing stiffness $\overline{K}(\bar{t})$ to 99.7% of the nominal gear

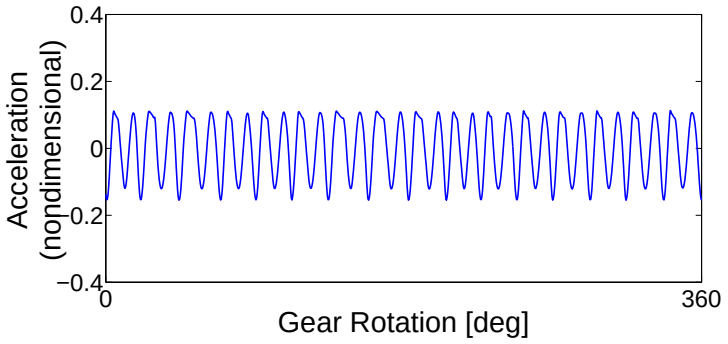

(a) Undamaged case, steady load condition.

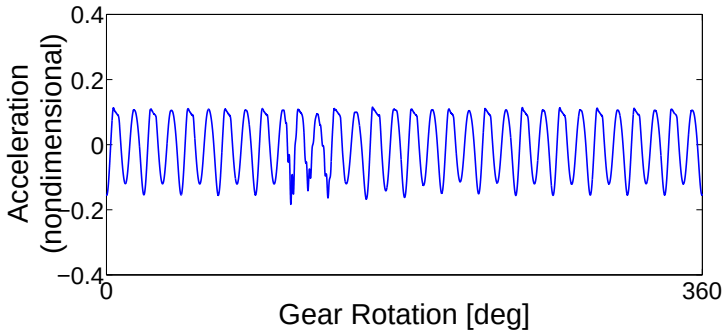

(b) Damaged case, steady load condition.

Figure 5: The acceleration diagrams of the simulation.

meshing stiffness for 5 degrees of the shaft rotation, periodically, for every rotation of the damaged gear. This was done in previous studies also, see Ref. [23]. Fig. 4 shows the reduction in stiffness for a tooth with crack. Figs. 5a and 5b show the acceleration diagrams of the simulation for the undamaged and damaged cases, for steady load conditions. The Fourier spectra of these diagrams are shown in Fig. 6, in *log* scale. The difference due to damage is subtle at the frequency range $0-2$. More apparent differences can be seen at the higher frequencies $(3-4)$.

2.5. Time-varying loads

Wind turbines undergo time-varying and transient load conditions, with load changes being far from smooth. To simulate these load conditions a series of wind turbine aerodynamics codes, developed by the National Renewable Energy Laboratory (NREL, US), is used in this work [36]. FAST is a design code written in FORTRAN that can be used to simulate wind turbine systems under a variety of operating conditions, including conditions related to wind speed variation and turbulence, and generator start-ups and

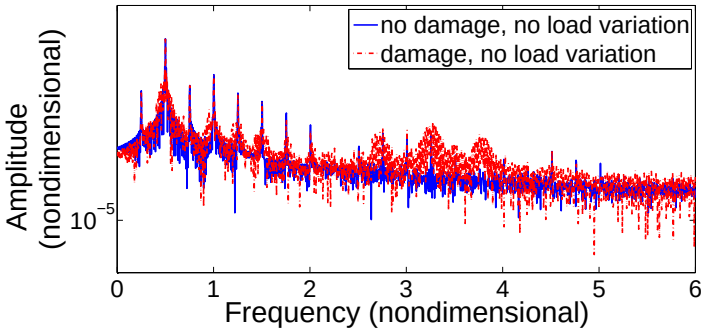

Figure 6: The Fourier Spectra of the simulation undamaged and damaged cases for $\overline{T}_{1var}(\bar{t}) = 0$ (steady load conditions).

shut-downs. Fig. 7 shows the load case examined in this work. Turbulent wind conditions are considered, with wind speed 12m/s.

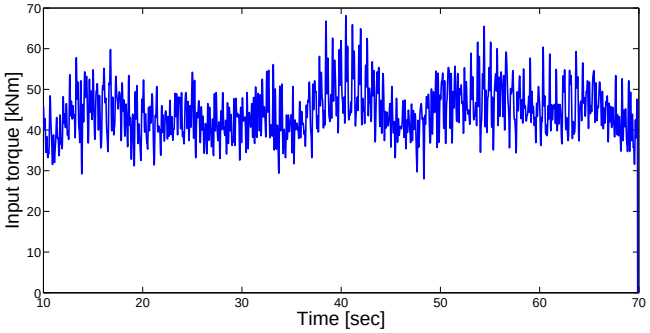

Figure 7: The high speed shaft torque for turbulent wind conditions (wind speed=12m/s, FAST simulation).

The load variation is shown in the time-acceleration plot as an increase in the acceleration amplitude when the sudden load changes occur. Such a load creates a nonstationarity in the acceleration signal. Concerning the values of this input torque simulated in FAST, $\overline{T}_{1var}(\bar{t})$, they correspond to a different system produced in FAST. For this reason it was important to do a normalisation before inserting the load to the simulated gear model. The equations of this normalisation are described in Section 2.1. The acceleration diagram for the undamaged and damaged cases and varying load conditions is shown in Figs. 8a and 8b. The influence of the time-varying load on the acceleration diagrams can be observed since the signals have become evidently less smooth and more nonstationary. Moreover, the effect of damage is harder to see in the acceleration signal, Figs. 8a and 8b, compared to the previous example. The Fourier spectra of these signals for the damaged and the undamaged cases are also given in Fig. 9. The differences here between the damaged and undamaged cases are not as clear as for the steady load

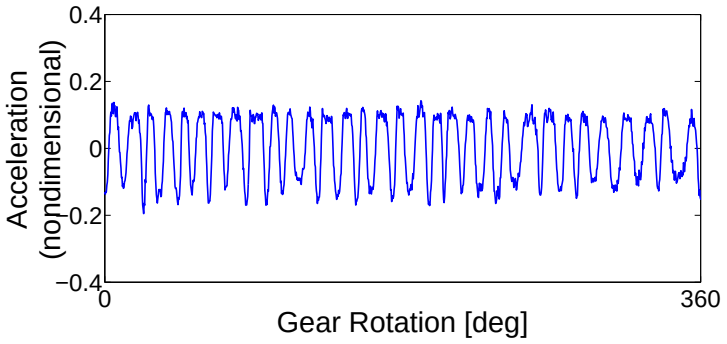

(a) Undamaged case, varying load condition.

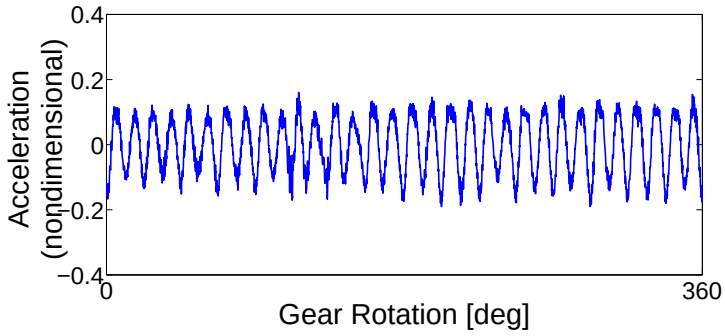

(b) Damaged case, varying load condition.

Figure 8: The acceleration diagrams of the simulation.

simulation given in Fig. 6. Under these circumstances, it is even harder to detect damage in its early stages using conventional vibration monitoring techniques. The results presented, are a very basic comparison of course and cant represent or prove that every conventional vibration monitoring technique, such as for example the time synchronous averaging, would fail. These figures succeed more in showing that varying operational effects can affect the signals in a way that could inhibit the performance of such techniques that might still work of course for some cases-but not always. That is why a time-frequency approach is proposed in this paper.

3. Wind turbine experimental data

The experimental measurements have been taken by members of the company EC Grupa, a Polish engineering company that maintains the wind turbine system from which the gearbox vibration datasets were obtained. The experimental gearbox vibration data analysed in this study come from

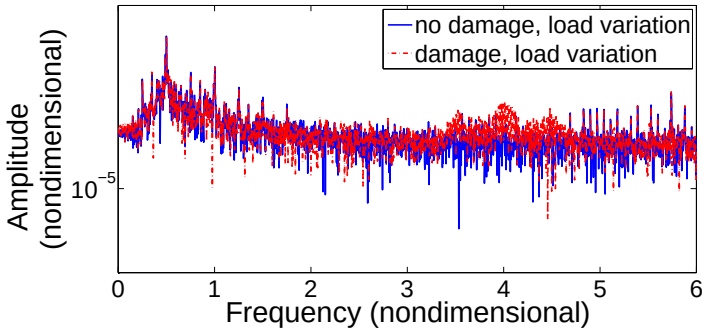

Figure 9: The Fourier Spectra of the simulation undamaged and damaged cases for the varying load condition.

an NEG Micon NM 1000/60 wind turbine in Germany. The gearbox is described by the kinematic scheme shown in Fig. 10.

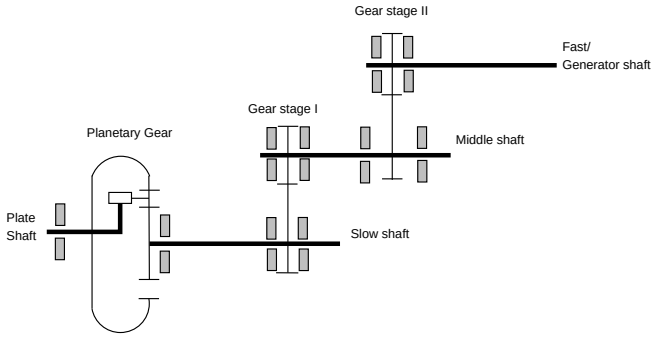

Figure 10: Kinematic scheme of the wind turbine gearbox.

The measurements come from a single accelerometer with sampling frequency 25000 Hz.

Acceleration signals from this gearbox were obtained at three different dates: 31/10/2009, 11/2/2010 and 4/4/2010. The first dataset was described as the one to be used as a reference. This is sensible because we expect damage to increase. If it transpired that the system was undamaged at the first test, then one would see clear signatures of damage in the later data. If it transpired that damage was already present during the first test, one can still use it as a reference and look for increased signatures of damage. The second dataset was considered to be one describing an early tooth damage of the gearbox and the third one was the dataset of the vibration signal with progressed tooth damage in the gearbox.

The kinematic scheme of the gearbox shows that it has two parallel spur gear stages and one planetary gear stage. When a gearbox has two or more mesh stages, signal processing of its vibration signals becomes more challenging because there are multiple shaft speeds and meshing frequencies apart

from noise. This means, for the case of gear tooth damage, that one should examine the specific frequencies associated with the meshing frequencies and their harmonics of the specific stages that include the damaged gears. Without analysing the data, one could probably make an initial assumption of the frequency bands that will be affected by damage, based on the fact that the damage was located at the second parallel gear stage, as will be briefly described later on. In this case, one should expect damage features at the highest frequency components (excluding noise) of the signal since the second parallel gear stage includes the fast generator shaft and because generally, it is known that it is in the harmonics of the meshing frequency of the damaged gear pair that damage features occur.

Fig. 11a shows the time domain signal of the dataset obtained on 4/4/2010. The gearbox examined has a 28-tooth gear (smaller wheel) that meshes with an 86-tooth gear (bigger wheel) at the parallel gear stage II, which is the one at which damage was observed.

The frequency components of the signal, as shown in the acceleration spectrum, Figs. 11b and 11c, are the following:

- 15.07, 30.14 Hz: relative meshing frequency and second harmonic of the planetary gear,
- 89.535, 179.07 Hz: relative meshing frequency and second harmonic of the 1^{st} parallel gear stage,
- 352, 705, 1410, 2115, 2820 Hz: relative meshing frequency and harmonics of the 2^{nd} parallel gear stage,
- Noise.

4. Signal processing methods

4.1. Empirical mode decomposition

In order to isolate the frequencies of interest when analysing a signal, bandpass filtering is needed. In this way one can exclude parts of the vibration signal not associated with the particular component examined, in this case the gearbox. Also for the case of multistage gearboxes, where the vibration signals are influenced by the meshing frequencies and harmonics of the different stages, the application of filter banks is useful. The EMD method decomposes the time-domain signal into a set of signal components (oscillatory functions) in the time-domain called intrinsic mode functions (IMFs). Each IMF is associated with a frequency band of the signal, so the EMD method is a filter bank method, and can be used for isolating unwanted components of the signals being analysed. By definition, an IMF should satisfy the following conditions [11]: (a) the number of extrema and

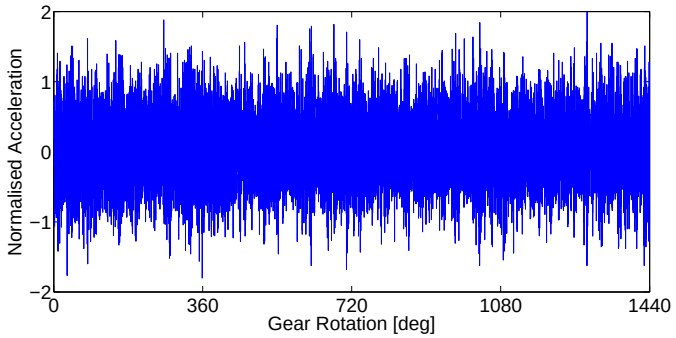

(a) Time history signal of acceleration (data set 4/4/2010).

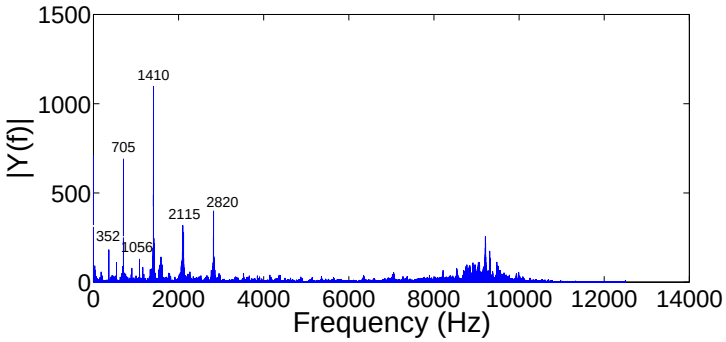

(b) Fourier spectrum of the signal shown in Fig. 11a

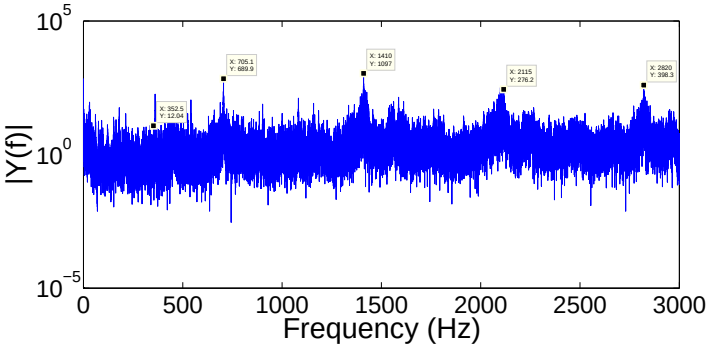

(c) Detail of the Fig. 11b (*log* scale).

Figure 11: Gearbox data of the NEG Micon NM 1000/60 wind turbine.

the number of zero crossings over the entire length of the IMF must be equal or differ at most by one, and (b) at any point, the mean value of the envelope defined by the local maxima and the envelope defined by the local minima is zero. The EMD method is well known now, but the theory is added here for completeness. The EMD decomposition procedure for extracting an IMF is

called the *sifting process* and consists of the following steps:

1. The local maxima and the local minima of the signal $x(t)$ are found.
2. All the local maxima of the signal are connected to form the upper envelope $u(t)$, and all the local minima of the envelope are connected to form the lower envelope $l(t)$. This connection is usually made using a cubic spline interpolation scheme.
3. The mean value $m_1(t)$ is defined as:

$$m_1(t) = \frac{l(t) + u(t)}{2} \tag{15}$$

and the first possible component $h_1(t)$ is given by the equation:

$$h_1(t) = x(t) - m_1(t) \tag{16}$$

The component $h_1(t)$ is accepted as the first component only if it satisfies the conditions to be an IMF. If it is not an IMF, the *sifting process* is followed until $h_1(t)$ satisfies the conditions to be an IMF. During this process $h_1(t)$ is treated as the new data set, which means that its upper and lower envelopes are formed and the mean value of these envelopes, $m_{11}(t)$, is used to calculate a new component $h_{11}(t)$ hoping that it satisfies the IMF criteria:

$$h_{11}(t) = x(t) - m_{11}(t) \tag{17}$$

The *sifting process* is repeated until the component $h_{1k}(t)$ is accepted as an IMF of the signal $x(t)$ and is denoted by $C_1(t)$:

$$C_1(t) = h_{1k}(t) = h_{1(k-1)}(t) - m_{1k}(t) \tag{18}$$

4. The first IMF is subtracted from the signal $x(t)$ resulting in the residual signal:

$$r_1(t) = x(t) - C_1(t) \tag{19}$$

During the *sifting process* the signal $x(t)$ is decomposed into a finite number N of intrinsic mode functions and as a result N residual signals are obtained. The residual signal is used as the new data set for subsequent steps in the sifting process. The process ends when the last residual signal, $r_N(t)$ is obtained and is a constant or a monotonic function. The original signal $x(t)$ can be exactly reconstructed as the sum:

$$x(t) = \sum_{j=1}^{N} C_j(t) + r_N(t) \tag{20}$$

The EMD method is purely an empirical procedure, not a mathematical transformation. The method's main advantage compared to most previous methods of data analysis is that it is an adaptive method based on and derived from the data. In deterministic situations the EMD method proves really efficient as a decomposition method. In stochastic situations involving noise the EMD method is basically a dyadic filter bank resembling those involved in wavelet decomposition [41, 42]. The difference between them is that the EMD is a signal-dependent time-variant filtering method that creates modes and residuals that can intuitively be given a "spectral" interpretation, different to a pre-determined subband filtering method, like the wavelet transform [42]. So when the method works well, it has the advantage of decomposing the signal into a smaller number of meaningful signal components; when it does not, problems known as "mode mixing" can occur [43]. "Mode mixing" is defined as any IMF consisting of oscillations of dramatically disparate scales, caused most of the times by intermittency of the driving mechanisms. So in that case different physical processes can be represented in one mode. Still, as it will be shown, even with this problem, the EMD method proves efficient for damage detection.

4.2. The mode mixing problem of the EMD

What will follow is not a theoretical explanation of mode mixing but rather an attempt to show when this phenomenon is encountered and how it is exhibited when implementing the EMD algorithm, using some simulation examples. Since there exists no theoretical explanation of the EMD, it is quite difficult to theoretically explain the mode mixing problem as well, but one can find studies [43] that try to give a more in-depth description of the phenomenon, and propose solutions to it. As a matter of fact the simulations that follow are similar to some of the examples given in [43], but adjusted in order to fit the analysis of the kind of signals that will be encountered later when analysing the gearbox datasets. In that paper, in an attempt to explain the mode mixing problem, data with a fundamental part as a low-frequency sinusoidal wave with unit amplitude were simulated and at the three middle crests of the low-frequency wave, high-frequency intermittent oscillations with an amplitude of 0.1 were added riding on the fundamental. It was shown there that because of the steps followed in the sifting process, the upper envelope resembled neither the upper envelope of the fundamental (which is a flat line at unity) nor the upper one of the intermittent oscillations (which is supposed to be the fundamental outside intermittent areas). Rather, the envelope is a mixture of the envelopes of the fundamental and of the intermittent signals that led to a distorted envelope mean. Consequently, the initial guess of the first IMF is the mixture of both the low-frequency fundamental and the high-frequency intermittent waves.

Here, a similar simulation will be shown. The lower frequency fundamental wave will be a sum of sinusoids, described by the equation:

$$x_{fundamental} = 0.5t + sin(\pi t) + sin(2\pi t) + sin(6\pi t) \tag{21}$$

while the intermittencies, will be Gaussian modulated sinusoidal pulses (Matlab function *gauspuls.m*). The reason for using such kinds of intermittencies in the simulation is the fact that gear tooth damage and damage in bearings most of the time appears as impulses in the acceleration signals. At first the simulation was performed without adding any noise to the signals. The first steps of the sifting process are shown in Figs. 12a and 12b, where it is obvious that what was claimed in [43] is true. When intermittencies exist in the simulation, the mean envelope produced is influenced by both the envelopes of the fundamental and of the intermittent signals, indeed.

What will be of more interest in the current study though, is the number of IMFs produced in the simulations shown, and the frequency content of each IMF. The PSD of the signals of Figs. 12a and 12b, is given in Fig. 13. It is apparent there that the signal contains a lower frequency fundamental, for both simulations. The existence of intermitencies creates some higher frequency components.

After having applied the EMD algorithm to the previously described datasets, two IMFs were produced for the first case and six IMFs for the second case. This is shown in Fig. 14. The number of IMFs produced is influenced by the number of runs of the algorithm needed by the sifting process in order to produce a residual signal (constant or monotonic function). Since mode mixing is the reason that, during the first steps of the sifting process, the highest and the lowest frequency parts of the signal are not separated, but carried to the next modes, one could claim that mode mixing could be an additional cause of the production of a higher number of IMFs during the decomposition, which is actually confirmed by the simulation results given in this case.

The result of mode mixing is shown in Fig. 15, where the PSD of the first three IMFs is given. It is obvious here that these modes have coinciding frequency bands.

This problem seems to be improved when using a "noise assisted data analysis" approach to the EMD, the EEMD, and several studies have focused on the performance of the EMD algorithm in the presence of noise, [42, 43]. If the decomposition is insensitive to added noise of small amplitude and bears only little changes, the decomposition is generally considered stable and satisfies a condition of physical uniqueness; otherwise, the decomposition is unstable and does not satisfy physical uniqueness. From this point of view, the EMD is considered an unstable technique, since due to mode mixing any perturbation can result in a new set of IMFs as reported by [44].

For deterministic signals, or even signals that may contain a reasonable amount of noise, any additional signal components should result in

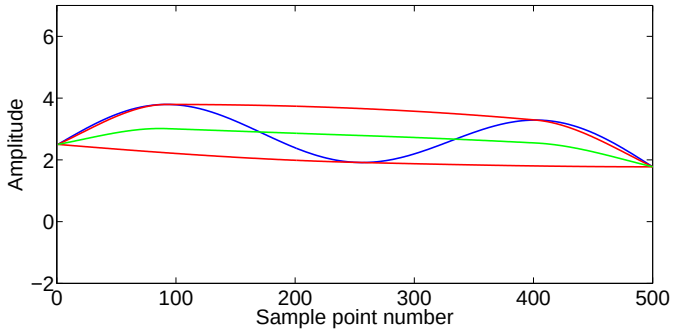

(a) A signal containing no intermittencies.

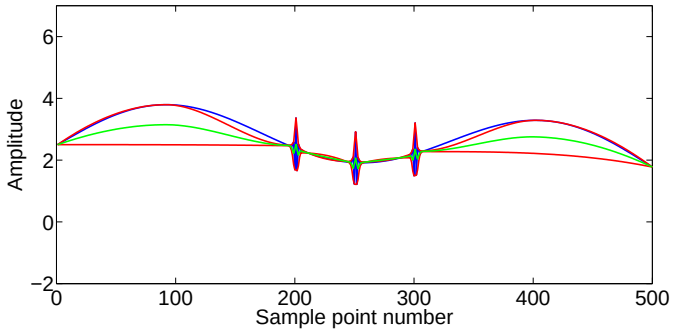

(b) A signal containing intermittencies.

Figure 12: Illustration of the first steps of the sifting process. The blue line shows the signal, the red lines the upper and lower envelopes and the green line the mean value of the envelopes.

additional IMFs (since the algorithm is supposed to decompose signals into meaningful signal components). If the signal does not contain any noise and has intermittencies then an even higher number of IMFs may be expected. Because noise seems to solve the mode mixing problem, if the signal contains a certain amount of noise, then additional components would result in additional IMFs again, but this time mode mixing might or might not occur, depending on the amount of noise the signal contains and the kind of intermittency. This will be shown in the next simulation.

When analysing Gaussian noise with the EMD, it is worth mentioning that as already proved in [42], the EMD method acts as a dyadic filter bank. In that case a specific number of IMFs with overlapping frequency bands will be created. It is generally believed that noise seems to fix the mode-mixing problem.

In order to have an idea of how the addition of noise would influence the previous simulation, the same datasets are used again in the next example (Figs. 16a and 16b), this time after having added Gaussian noise with a signal-to-noise ratio of 25. The number of IMFs produced in this

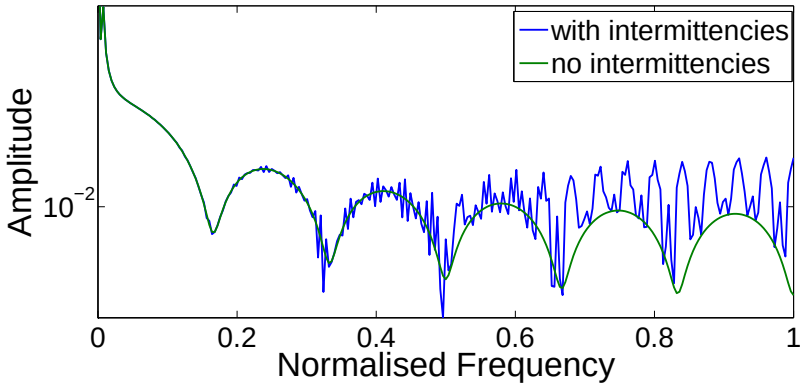

Figure 13: The PSD of the signals of Figs. 12a and 12b.

case is six for the first dataset that does not contain the intermittencies and eight for the dataset that contains the intermittencies (Fig. 17). The existence of noise in the datasets has generated a higher number of IMFs, but again for the signal that contained the Gaussian modulated sinusoidal pulses (intermittencies), even more IMFs were produced. So it is obvious from this simulation that the addition of impulses in a signal that contains a little noise will add again additional IMFs when performing the EMD method. The results presented here are by no means a theoretical proof of how the mode mixing problem affects the EMD analysis in general, as already mentioned previously reference [43] has a more theoretically thorough explanation of the mode mixing effect on the EMD method. The simulations presented here rather aim to help the reader understand what could be expected in the results of the analysis in this case. Finally, Fig. 18 shows the frequency content of the first three IMFs of the second signal, the one that contains the intermittencies, in order to have a better demonstration of different frequency regions that these three IMFs contain.

4.3. The Hilbert transform

The HT is a linear integral operator [45]. It can be used to derive the analytic representation of the signal $x(t)$. The analytic representation of a signal facilitates the estimation of the instantaneous amplitude and frequency of a signal. If $\hat{x}(t)$ is the HT of a signal $x(t)$, it is given by the equation:

$$\hat{x}(t) = \frac{1}{\pi} \int_{-\infty}^{+\infty} \frac{x(\tau)}{t-\tau} \, \mathrm{d}\tau = x(t) * \frac{1}{\pi t} \tag{22}$$

Given $\hat{x}(t)$ one can define the analytic signal, introduced by [46]:

$$z(t) = x(t) + i\hat{x}(t) \tag{23}$$

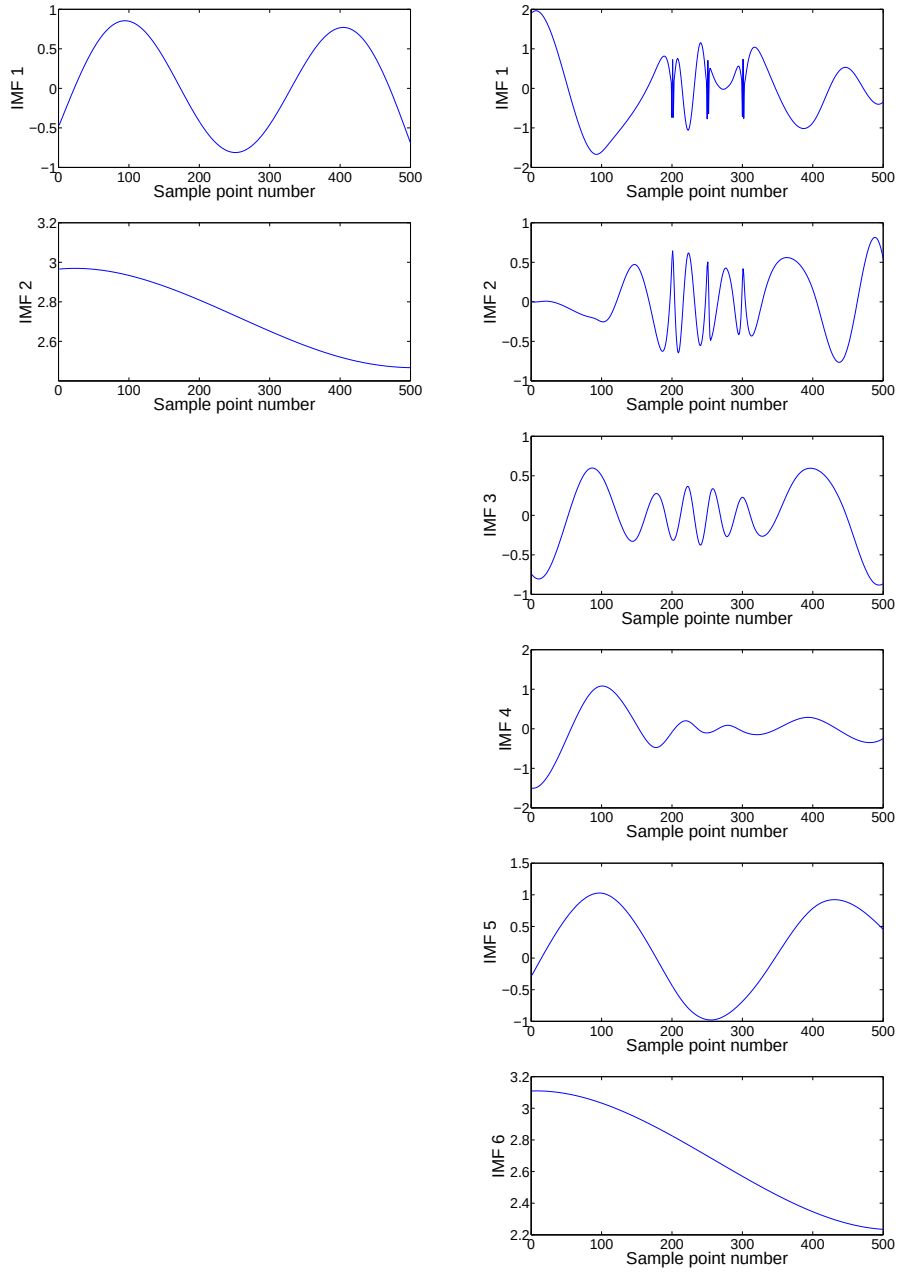

(a) (b)

Figure 14: IMFs of the signals shown in Figs. 12a and 12b. More particularly: (a) IMFs of signal with no intermittencies (blue line of 12a (a)) and (b) IMFs of signal with intermittencies (blue line of 12b (b)).

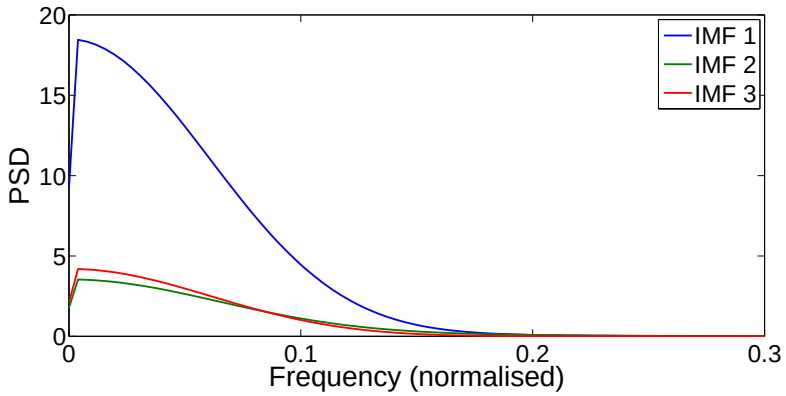

Figure 15: The PSD of the first three IMFs of the second signal (that contains intermittencies).

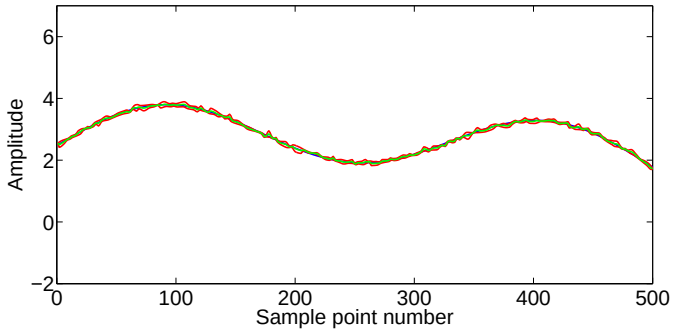

(a) A signal containing Gaussian noise and no intermittencies.

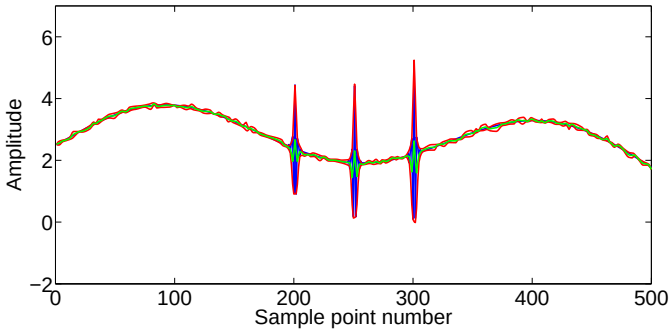

(b) A signal containing Gaussian noise and intermittencies.

Figure 16: Illustration of the first steps of the sifting process. The blue line shows the signal, the red lines the upper and lower envelopes and the green line the mean value of the envelopes.

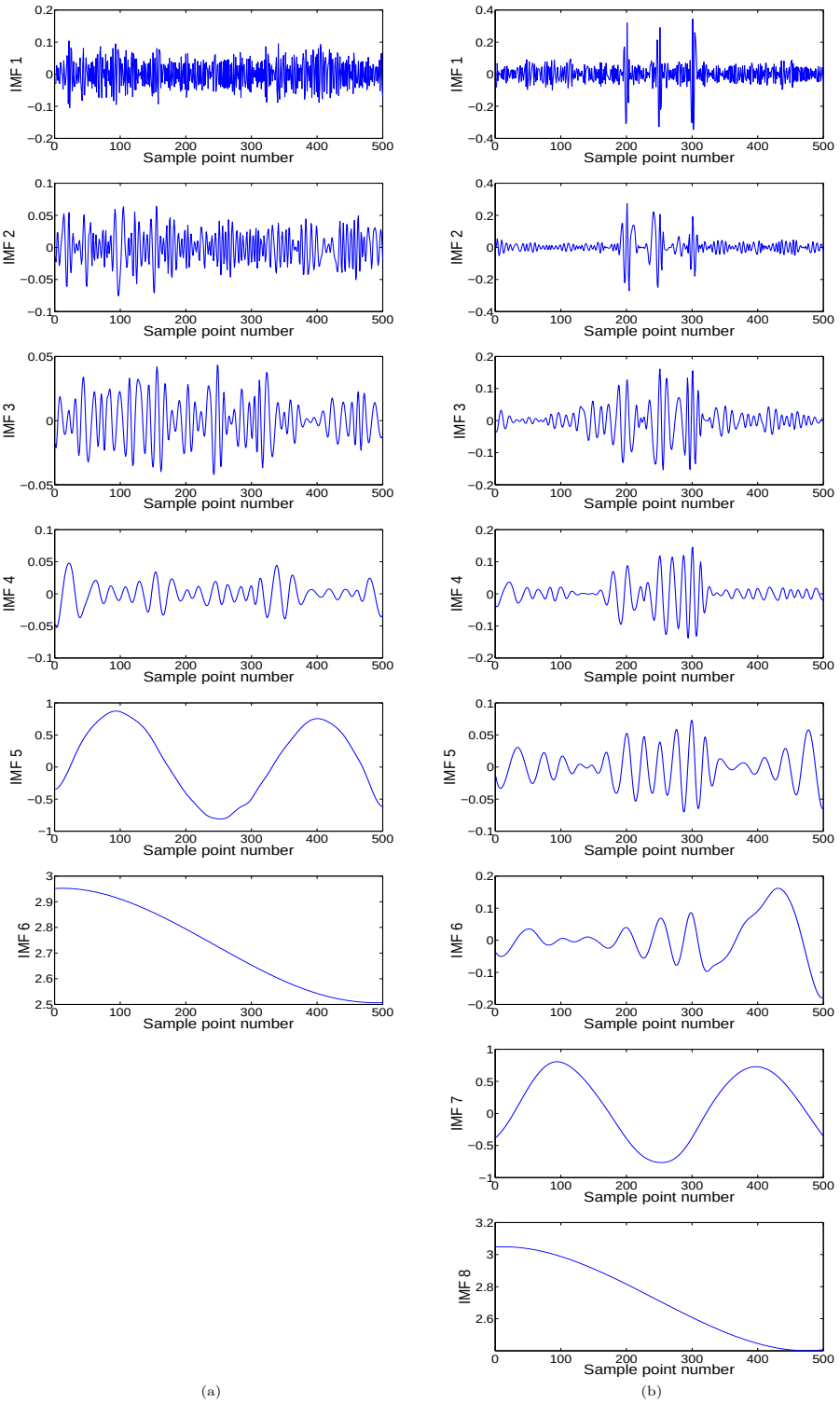

Figure 17: IMFs of the signals shown in Figs. 16a and 16b. More particularly: (a) IMFs of signal with no intermittencies (blue line of 16a) and (b) IMFs of signal with intermittencies (blue line of 16b).

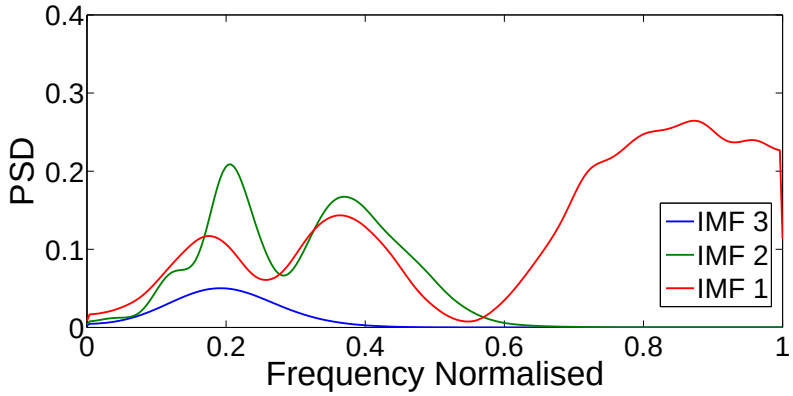

Figure 18: The PSD of the first three IMFs of the second signal (that contains intermittencies).

where i is the imaginary unit. The equation (23) written in its exponential form gives:

$$z(t) = A(t)e^{i\theta(t)} \tag{24}$$

where $A(t)$ is the amplitude envelope of the signal, and $\theta(t)$ the instantaneous phase. The amplitude envelope and instantaneous phase can be estimated by the following equations:

$$A(t) = \sqrt{x(t)^2 + \hat{x}(t)^2} = |z(t)| \tag{25}$$

$$\theta(t) = arctan(\hat{x}(t)/x(t)) = Arg(z(t)) \tag{26}$$

and the instantaneous frequency can be calculated by:

$$f(t) = \frac{1}{2\pi}\frac{d\theta(t)}{dt} \tag{27}$$

Combining the above with the EMD method, the original signal $x(t)$ can be expressed as:

$$x(t) = Re\{\sum_{j=1}^{N} A_j(t)e^{i\int \omega_j(t)dt}\} \tag{28}$$

where j is the number of the IMFs and A_j and ω_j the instantaneous amplitude and instantaneous angular frequency of the j^{th} IMF. The above equation enables one to represent the instantaneous amplitude and instantaneous frequency of the signal in a three-dimensional plot. This time-frequency representation is designated as the Hilbert spectrum.

The FT of equation (22) gives:

$$\hat{X}(\omega) = X(\omega)(-jsgn(\omega)) \tag{29}$$

Equation (29) shows that the HT can be estimated in a more simple way: by transforming the signal into the frequency domain, and shifting the phase of positive frequency components by $-\pi/2$ and of negative components by $+\pi/2$ and then transforming back to the time-domain. So two important properties of the HT are:

- the HT preserves the domain in which the signal is defined,
- the HT shifts the phase of the signal by 90°.

The HT is estimated in the following analysis using the Matlab function *hilbert.m*. The algorithm used in order to compute the HT uses the following steps.

- The Fast Fourier Transform (FFT), of the input sequence is calculated, storing the result in a vector x.
- A vector h (Hilbert window) is created. The elements of this vector ($h(i)$) have the values:
  - 1 for $i = 1, (\frac{n}{2}) + 1$
  - 2 for $i = 2, 3, \ldots (\frac{n}{2})$
  - 0 for $i = (\frac{n}{2}) + 2, \ldots, n$

  where n are the sample points.
- The element-wise product of x and h is calculated.
- The inverse FFT of the sequence obtained in the previous steps is calculated and the first n elements of the result are returned.

Estimating the instantaneous amplitude, after these steps is simple, since it is the amplitude of the complex Hilbert transform. The instantaneous frequency is the time rate of change of the instantaneous phase angle.

4.4. The Teager-Kaiser energy operator and the energy separation algorithm

The Teager-Kaiser energy operator (TKEO), can estimate the instantaneous "energy" of a signal, and it is defined as:

$$\Psi_c[x(t)] = [\dot{x}(t)]^2 - x(t)\ddot{x}(t) \tag{30}$$

where $x(t)$ is the signal and $\dot{x}(t)$ and $\ddot{x}(t)$ are its first and second derivatives respectively. In the discrete time case, the time derivatives in equation (30) can be approximated by time differences:

$$\Psi_d[x(n)] = x(n)^2 - x(n+1)x(n-1) \tag{31}$$

The TKEO offers excellent time resolution because only three samples are required for the energy computation at each time instant. The operators Ψ_c and Ψ_d were developed by Teager during his work on speech production modelling [14, 15] where he described the nonlinearities of speech production and showed a plot of "the energy creating sound", without giving though the algorithm to calculate this "energy". Later, Kaiser presented the algorithm developed by Teager in his work [16, 17].

An alternative approach to that of the Hilbert transform separation algorithm for the estimation of instantaneous envelope $A(t)$ and instantaneous frequency of the signal $f(t)$, was developed in [47]. It uses the TKEO to estimate initially the required energy for generating the signal being analysed and then to separate it into its amplitude and frequency component using an energy separation algorithm.

The energy separation algorithm is described by the following equations:

$$f(t) = \frac{1}{2\pi}\sqrt{\frac{\Psi[\dot{x}(t)]}{\Psi[x(t)]}} \tag{32}$$

$$|A(t)| = \frac{\Psi[x(t)]}{\sqrt{\Psi[x(t)]}} \tag{33}$$

These equations estimate exactly the instantaneous frequency and amplitude envelope of a sinusoidal signal, and the approximation errors for the cases of amplitude modulation (AM), frequency modulation (FM) and AM-FM signals are small [48]. There have been developed several discrete time energy separation algorithms; here Desa-1 is given [47]:

$$arccos(1 - \frac{\Psi_d[y(n)] + \Psi_d[y(n)]}{4\Psi_d[x(n)]}) \approx f_i(n) \tag{34}$$

$$\sqrt{\frac{\Psi_d[x(n)]}{1 - (1 - \frac{\Psi_d[y(n)]+\Psi_d[y(n+1)]}{4\Psi_d[x(n)]})^2}} \approx |A(n)| \tag{35}$$

where $x(n)$ is the signal and $y(n) = x(n) - x(n-1)$ is its backward asymmetric difference and if T is the sampling period:

$$F_i = f_i T \tag{36}$$

The frequency estimation part assumes that $0 < F_i(n) < \pi$ which means that the algorithm can estimate frequencies up to $1/2$ the sampling frequency. This is due to the fact that the sine function and its inverse have a unique correspondence between 0 and $\pi/2$. Since the sine argument is $F_i/2$, it follows that the frequency can be uniquely determined for any F_i between 0 and π. A simple simulated example in order to show the performance of both the Hilbert Transform and the TKEO/ Desa-1 approach is given here.

The instantaneous frequency and amplitude envelope of a chirp signal, Fig. 19, are calculated using both methods. The results, Figs. 20a, 20b, 21a and 21b show that both methods have almost the same resolution with the energy separation method doing a little better.

The reason that the results of the HT show a worse end-effects problem is related to a circular convolution issue, [49]. This problem could probably be solved if one chose to zero-pad or truncate the data analysed. This could also improve the resolution of the method although it would make the algorithm a little slower. Since the analysis of the experimental data did not show similar problems, as will be shown later, because the variations in the signals were not as dramatic as the variation in the simulated chirp, this problem is not of major importance in the current study.

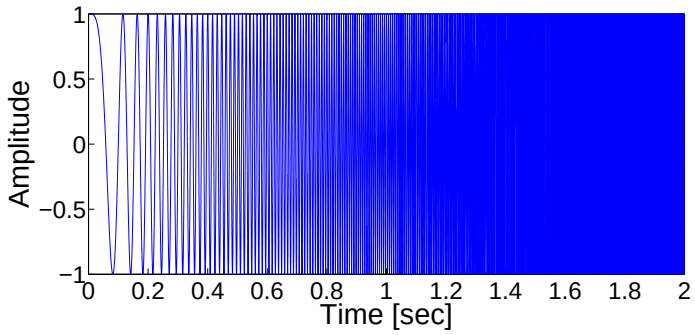

Figure 19: Chirp signal.

The main problem that occurs during the estimation of the instantaneous characteristics of the signal being analysed, using both methods, is that a differentiation exists in the process. This is the reason why signals with low signal to noise ratio cannot be analysed efficiently, since differentiation amplifies noise. So applying an appropriate filter before the estimation of the instantaneous characteristics, in order to denoise the signal, is important. More particularly, the TKEO can only be applied to monocomponent signals, so a filter bank method should first be applied to the signal analysed in order to extract its monocomponents and analyse them separately with the TKEO/ Desa-1 approach. In this case, the EMD method is the filter bank method applied. In addition, one should pay attention to having signals that are smooth enough for both of the amplitude-frequency separation approaches, since differentiation may produce spikes at the points where the signal is not smooth. For this reason, a cubic spline interpolation in the EMD sifting process is preferred, as opposed to a linear interpolation which would not produce smooth IMFs, and also a smoothing filter should be applied to the IMFs produced before the estimation of their instantaneous characteristics.

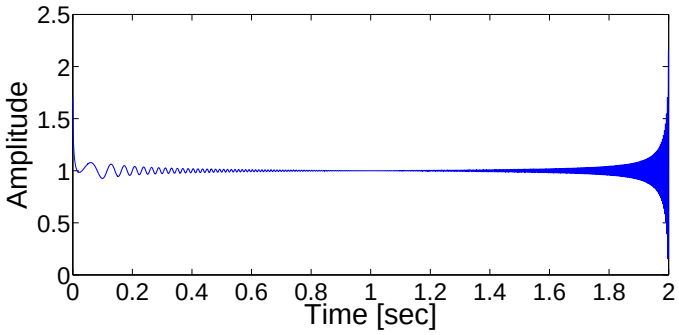

(a) Results obtained using the HT.

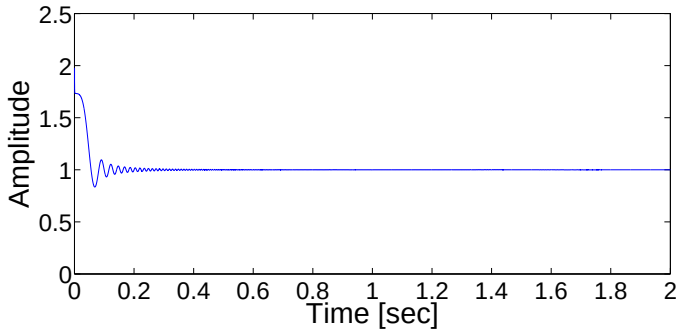

(b) Results obtained using the TKEO and Desa-1.

Figure 20: Chirp signal amplitude envelope using the two different amplitude-frequency demodulation approaches.

5. Results

5.1. Simulation results - how the EMD works

Fig. 23, displays the results of the EMD on the simulated vibration signals given in Figs. 22a, 22b and 22c which correspond to three different cases. The first case is a simulation under steady load conditions and without any tooth damage in the gear model. The second case is a simulation under time-varying load, produced in FAST and without any tooth damage in the gear model. Finally, the third case is the simulation under time-varying load and with an early damaged tooth. The diagrams represent three gear revolutions. One can observe that the first case produced has the smallest number of IMF signal components. The application of time varying load in the model created effects in the signal that were recognised by the EMD algorithm as more signal components than the previous case; that is the reason why this time one more IMF was extracted. Finally, the introduction of damage created three more IMFs than the second case. The reason that three more IMFs were produced in this case, instead of just one, is related

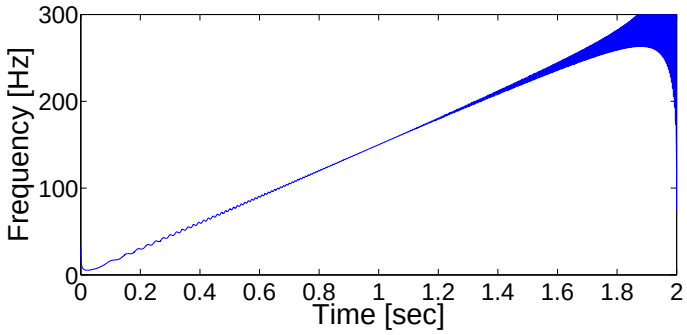

(a) Results obtained using the HT.

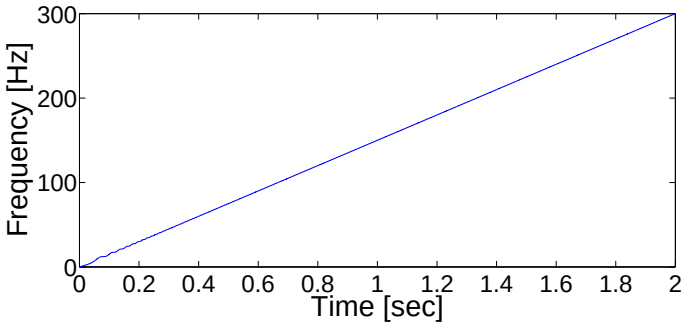

(b) Results obtained using the TKEO and Desa-1.

Figure 21: Chirp signal instantaneous frequency using the two different amplitude-frequency demodulation approaches.

to the "mode mixing" problem discussed in sections 4.1 and 4.3. Basically, IMFs 2, 3 and 4 contain the frequency region of the harmonics of the meshing frequency and include damage features that should probably be found in just one IMF and would be separated from the rest of the signal components if the EMD algorithm worked perfectly. Damage is shown in these IMFs as periodic pulses with the period of the revolution of the damaged gear. So damage is an intermittency in the vibration signal.

The best IMF representing the effects of damage visually (the pulses are more apparent) is IMF 3. The instantaneous characteristics of this IMF can give probably the best features for damage detection, although the analysis of the other two IMFs would give sufficient features also. The occurrence of the EMD's "mode mixing" problem, in the way that is shown in this simulation, suggests that further research might be of interest on whether the number of IMFs, for the case of gearbox signals that don't contain a significant amount of noise, can serve as one more indicator of damage, from the point of view that a higher number of IMFs might be produced in this case not only due to new frequencies in the signal related to damage

but also due to mode mixing.

This is an interesting observation that hasn't been found in other studies, that have treated the "mode mixing" as a disadvantage and have proposed improved methods of the algorithm for condition monitoring. Strictly speaking, "mode mixing" is indeed a problematic feature of the algorithm in signal processing terms, since it might reduce the resolution of the time-frequency analysis. Still, even under these circumstances, the EMD produces, if not better, at least equal results with other time-frequency methods, such as wavelets. All the above make the authors believe that there might be a potential in using this trait of the EMD as an indicator of damage, since damage is a form of intermittency in the vibration signals that could create a significantly higher number of produced IMFs.

Another observation is that the kind of time varying load used in these simulations has an effect on the first IMF of the signals. A major part of the load variation effect is decomposed in the first IMF of the decomposition and therefore identified mainly as "noise" or a high frequency component by the EMD method. It is important to say here, that the first IMF of each case represents a different frequency band. Basically, in the second and third cases examined, a high frequency component exists, influenced by the time-varying load, and represented by the first IMF, that does not exist in the first case, which is the steady load undamaged case. The second IMF of the second case, Fig. 23b, and the fourth IMF of the third case, Fig. 23c, are the equivalent to the first IMF of the first case, Fig. 23a. They represent the same frequency band, around the harmonics of the meshing frequency. And in a similar manner, the IMFs that follow for the three cases examined represent the same frequency bands of the signal. This is shown in Fig. 24a where the power spectral densities (PSDs) of the 1^{st} IMF of the first simulation, the 2^{nd} IMF of the second simulation and the 4^{th} IMF of the third simulation are compared and it is obvious that they fall in the same frequency bands. In the same manner the PSDs of the next two IMFs of each case are compared in Fig. 24b and 24c leading in the same conclusion. The effects of the time-varying load influence these frequency bands as well, still this will not create any problem in the damage detection part. The reason is mainly because the EMD algorithm manages to create an IMF representing the frequencies of damage effects in the vibration signal, in this case the IMF 3 of the third simulation, and isolates it from the rest of the signal components.

Finally, one should remember when proceeding in the analysis of the IMFs, that the first IMF represents the highest frequency component of the signal, and the ones that follow represent lower frequency components. So noise, which in this case has not been added to the signals, the harmonics of the meshing frequency of the gear model, the meshing frequency of the model and lower frequency components are represented in this particular order by the IMFs if they do exist in the signal. The same number of IMF doesn't

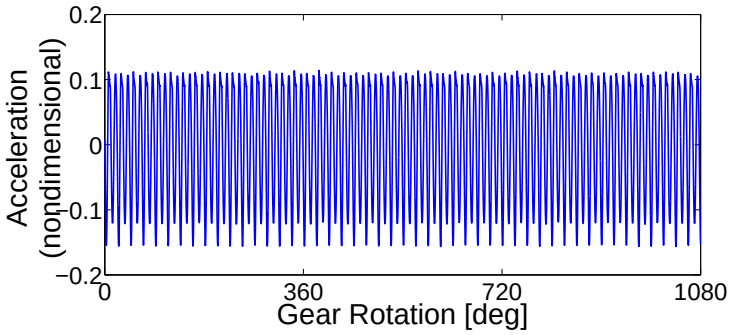

(a) Undamaged case - steady load.

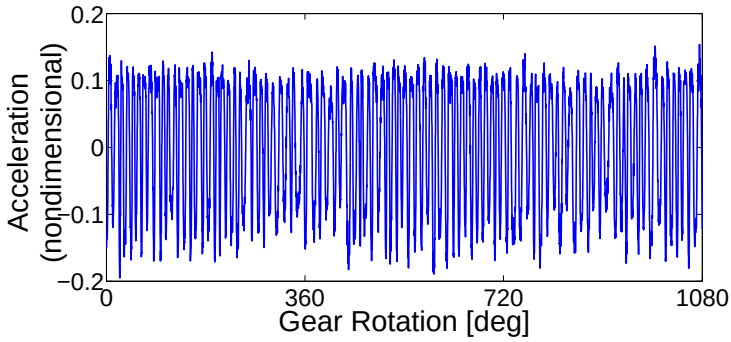

(b) Undamaged case - time-varying load.

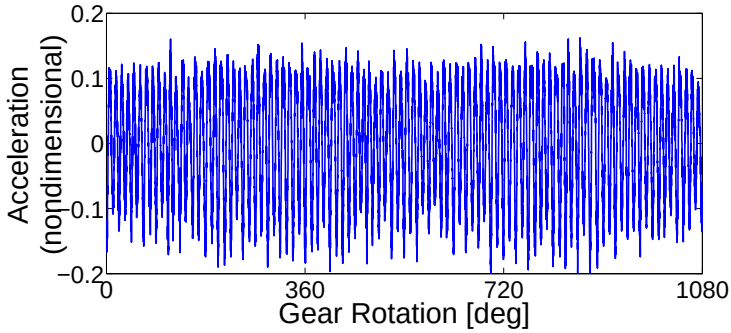

(c) Early damage in one tooth - time-varying load.

Figure 22: Acceleration diagrams of the simulations.

necessarily represent the same time-scale of the signal for the different cases examined. In addition, generally it is the first IMFs that will have damage indicators, since they represent the highest frequency components, and are more suitable for damage identification.

The amplitude-frequency separation of the third IMF of the third (damaged) case, using both approaches, the Hilbert Transform and the Teager

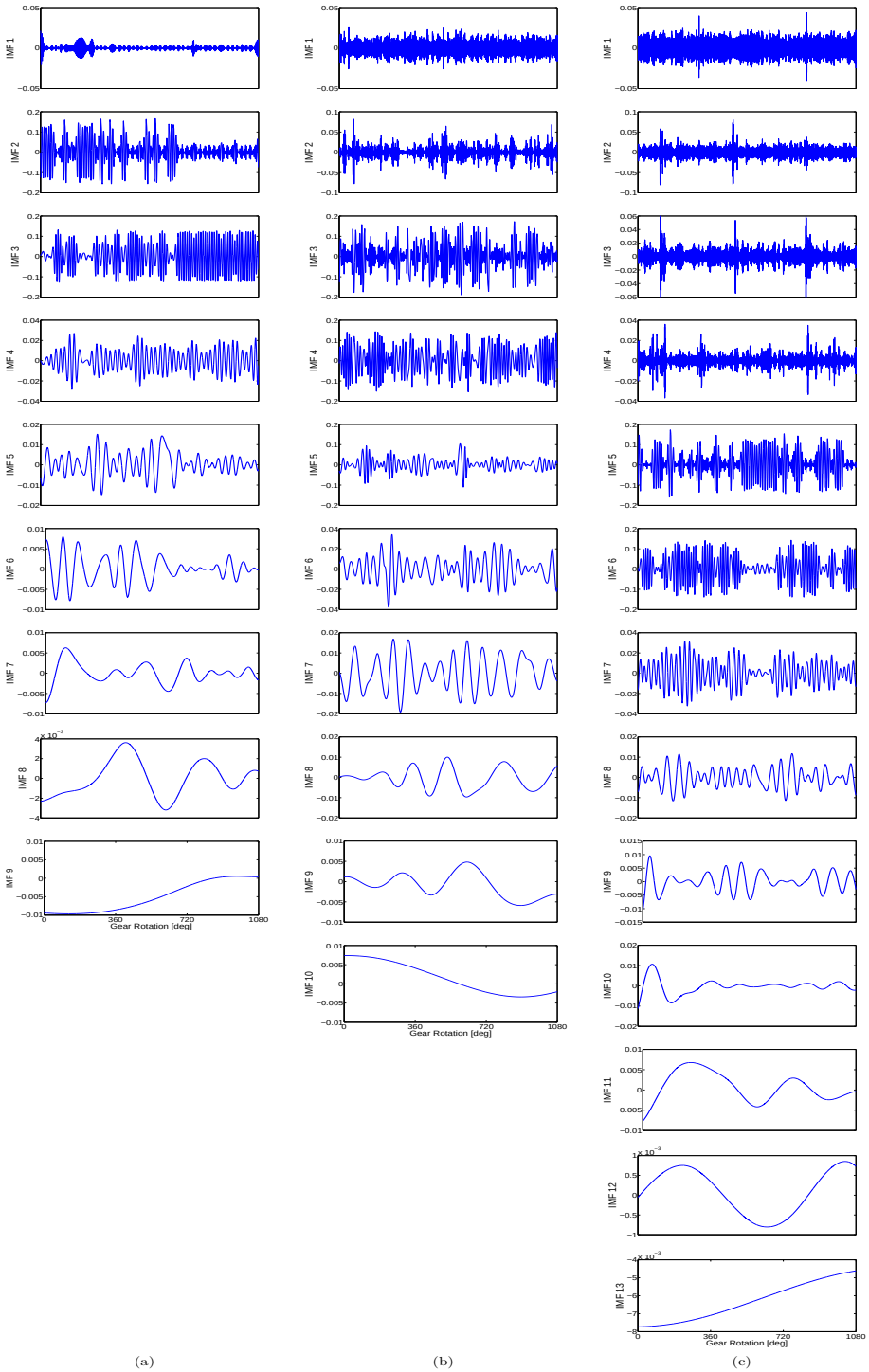

Figure 23: Intrinsic mode functions of simulations: (a) undamaged case - steady load, (b) undamaged case - time-varying load, and (c) early damage in one tooth - time-varying load.

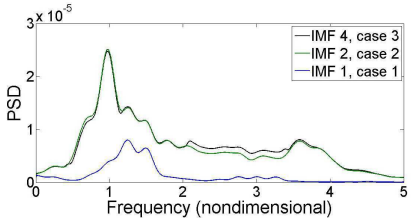

(a) 1^{st} IMF of the 1^{st} case, 2^{nd} IMF of the 2^{nd} case, and 4^{th} IMF of the 3^{rd} case.

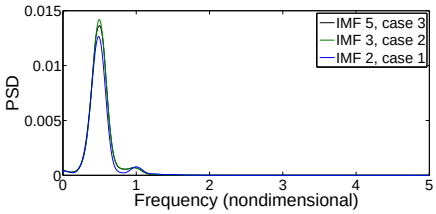

(b) 2^{nd} IMF of the 1^{st} case, 3^{rd} IMF of the 2^{nd} case, and 5^{th} IMF of the 3^{rd} case.

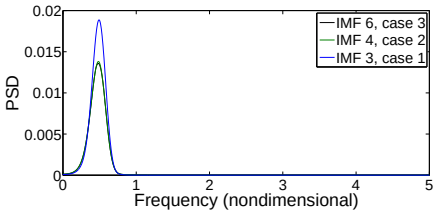

(c) 3^{rd} IMF of the 1^{st} case, 4^{th} IMF of the 2^{nd} case, and 6^{th} IMF of the 3^{rd} case.

Figure 24: PSD using the Welch method of the IMFs shown in Fig. 23.

Kaiser operator approach, is presented in this section. Both methods seem to have similar resolution in the frequency (Figs. 25a and 25b) and amplitude (Figs. 26a and 26b) diagrams. What is shown here is that the frequency of the third IMF, that was identified as the most sensitive to damage, drops at the point where the damage occurs, while the amplitude increases. The increase of the instantaneous amplitude can be explained due to the increase of the vibration levels when the damaged tooth engages. The instantaneous frequency, on the other hand, drops because the meshing stiffness drops and the compliance increases at that time. This happens because the damaged tooth is more flexible (more compliant) due to damage. Instantaneous frequency could be potentially used for diagnostics. The only restriction in this case could be that the estimation of frequency might be badly influenced by noise, but there exist simple solutions for this problem (filtering, which is what the EMD method does, and smoothing).

A measure of the power of the third IMF can be estimated according to

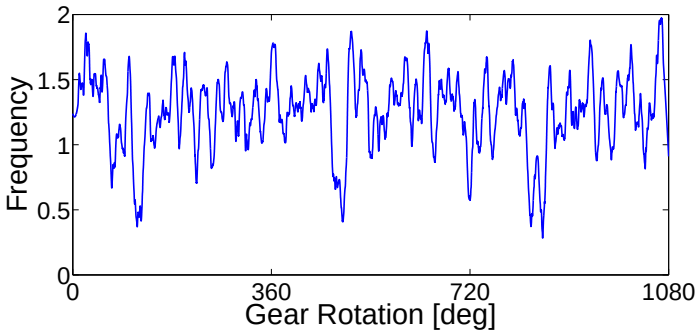

(a) Hilbert Transform results.

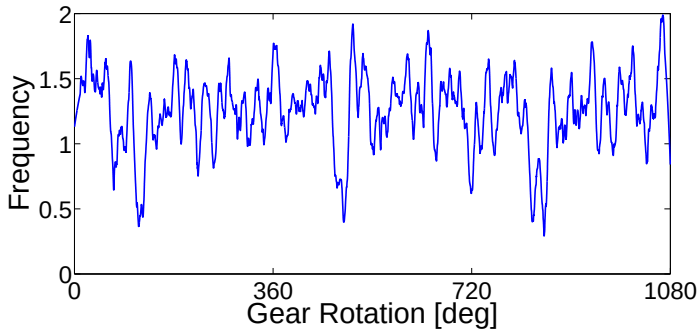

(b) TKEO and DESA-1 results.

Figure 25: Instantaneous frequency of the 3rd IMF of the third simulated case.

the equation:

$$P = \frac{1}{2} {A_i}^2(t) \tag{37}$$

where A_i is the instantaneous amplitude of the i^{th} IMF. This measure can be used to create the Teager Spectrum diagram that is shown later on in the experimental results. This power measure has nothing to do with the Teager "energy" that can be also estimated according to equation (30). In this way it is acceptable to make comparisons between the results that both methods produce.

5.2. Experimental data results

The three different datasets that were obtained from the wind turbine gearbox data were also decomposed using the EMD method and the results are shown in Fig. 27. The first dataset was decomposed into 13 IMFs, the second into 12 IMFs and the third into 13 IMFs. The diagrams represent four rotations of the smaller wheel of the parallel gear stage 2 (damaged gear). Small speed fluctuations might exist so the rotating period might not be exactly constant for the whole duration of the datasets.

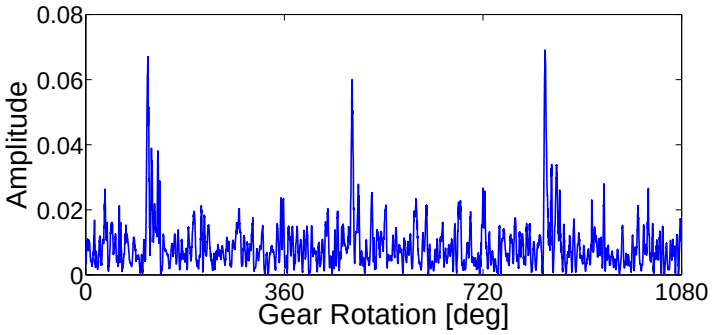

(a) Hilbert Transform results.

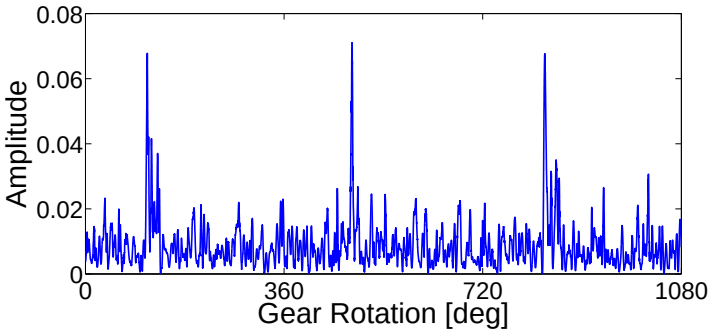

(b) TKEO and DESA-1 results.

Figure 26: Instantaneous amplitude of the 3rd IMF of the third simulated case.

Only the first four IMFs are presented here. The frequency content of each IMF is shown in Figs. 28a, 28b and 28c, that shows the PSD of all the IMFs for each dataset. The first four IMFs are the frequencies given by the dark blue, green, red and light blue lines in this figure (frequency domain). The first IMF is the highest frequency band of the signal (noise). The second IMF contains part of the fourth and the fifth meshing frequency harmonic (frequency band: 2500-5000 Hz). The third IMF contains mostly the third and part of the fourth meshing frequency harmonic (frequency band: 500-3000 Hz). The fourth IMF contains mostly the second meshing frequency harmonic (frequency band: 200-1500 Hz). The fifth IMF contains mostly the first meshing frequency harmonic-fundamental (frequency band: 150-600 Hz). The rest of the IMFs (not given here) are related to the meshing frequencies and harmonics of the other stages of the gearbox and to lower frequency components of the signals.

The tooth fault is most clearly shown in the second IMF as (almost) periodic pulses occurring at the time when the damaged gear (small wheel of the third gear stage) engages. The period of these pulses coincides with the rotating period of the damaged gear.

Periodic pulses can be seen but less clearly in the third IMF. Without proceeding to any further analysis, there is clearly some indication of damage in the first dataset which was initially considered to be describing the gearbox at an undamaged condition. This conclusion is drawn at this point by the fact that periodic pulses were produced in the second and third IMF of the first case as well. The EMD method produced 13 IMFs, which is the same number as the one produced in the third case, where damage was progressed, and one more in number than the number of IMFs of the second case.

The authors were informed after having performed the analysis that the first dataset, described as a reference dataset, was actually taken when the gearbox had already shown some first indications of damage. The authors were also informed that it is actually not easily feasible to obtain datasets of a gearbox during both its healthy condition and damaged condition. Collecting all vibration data of a healthy gearbox with the expectation that it might fail in the near, or not so near future, would mean that huge data storage is necessary.

A final remark concerning the influence of the varying load of the wind turbine gearbox will be given here. Despite the fact that the case examined here is concerning the third gear stage, which should not be as affected as the first gear stage, by the varying load caused by wind turbulences, the analysis of the experimental data shows that even this stage of the gearbox is influenced, underlying the importance of further examining the case of condition monitoring under varying load conditions. In this case a large part of the varying load influence on the vibration signals is carried in the first IMF, just as in the simulations, in addition to other types of noise that may exist in the wind turbine nacelle. Load variation due to wind turbulence influences mostly the highest frequency bands of the signal. Load variation may also be observed in other IMFs related to other frequency bands. The fact that the second case, dataset 11/2/2010, produced a lower number of IMFs than the other two, despite the fact that it was identified already by the condition monitoring systems of the wind turbine as describing a damaged gearbox, and therefore should have at least the same IMFs number as the first case, is probably explained by the different load conditions that may have existed at the specific measurements.

In fact, knowing now that the gearbox is damaged in all the datasets and since noise levels are high, means that this data cannot be used to support or contradict the hypothesis that damage could be reflected in the number of IMFs. Unlike the simulations, the experimental datasets all appear to have damage and have almost the same level of environmental loading. On the other hand, the data do not contradict the hypothesis. Further research is needed.

In order to obtain the amplitude envelope and the instantaneous frequency of the IMFs presented in the previous section, the IMFs were first

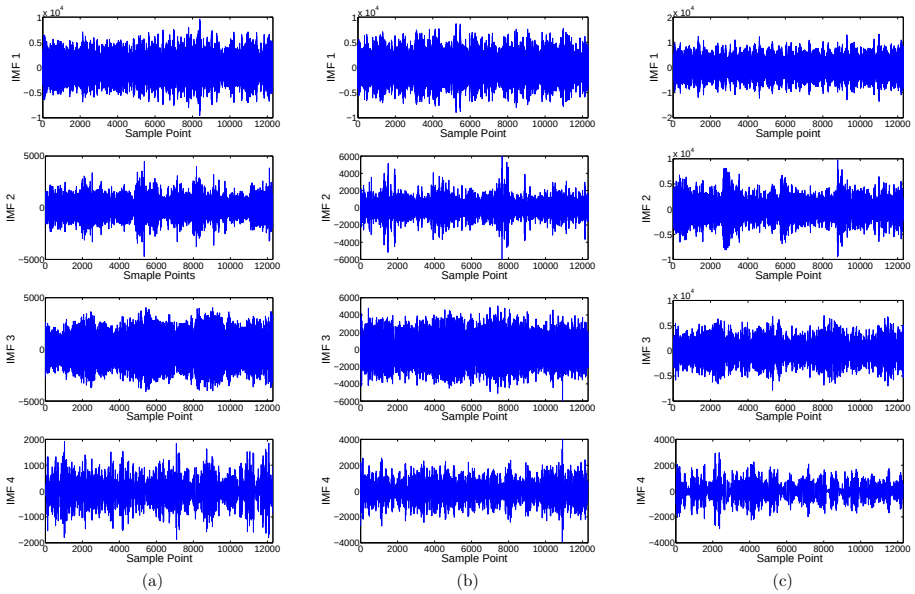

Figure 27: First four IMFs of the wind turbine gearbox data: (a) 31/10/2009, (b) 11/2/2010, and (c) 4/4/2010.

filtered with a smoothing filter (*sgolay* smoothing filter in Matlab). In this way, with the calculation of the instantaneous characteristics of the IMFs one can have the 3D diagrams of the signals, shown in Figs. 29a, 29b and 29c. Only the results obtained using the TKEO/ Desa-1 algorithms are shown here, since it was shown earlier that both the HT and the TKEO approaches give similar results in the simulations.

Damage has again the same pattern as in the simulations, so basically the frequency of the second IMF, which occupies the frequency band 2500-5000 Hz (roughly), drops each time that the damaged tooth engages (Figs. 29a, 29b and 29c). This is shown better in Figs. 30a, 30b and 30c where the instantaneous frequency diagram is plotted. This IMF represents the frequency band of the fifth harmonic of the parallel gear stage II (2820 Hz as mentioned earlier). The power levels increase at that specific time as well, Figs. 31a, 31b and 31c. As damage increases, the power levels increase and so the scales in the 3D diagrams increase. In addition, it is confirmed in this part of the analysis that there are some indications of damage in the first dataset too, and since it is at a relatively much lower power scale it must be at an early state.

A final remark that can be made here is related to the instantaneous frequency results. Generally fluctuations in speed lead to frequency modulation, while amplitude modulations are mostly related to load variations. Figs. 30a, 30b, 30c from this point of view suggests that there are speed variations too in the measurements that are possibly greater for the last

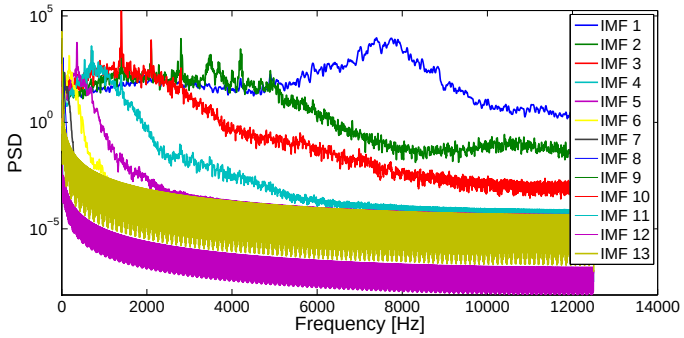

(a) Dataset 31/10/2009.

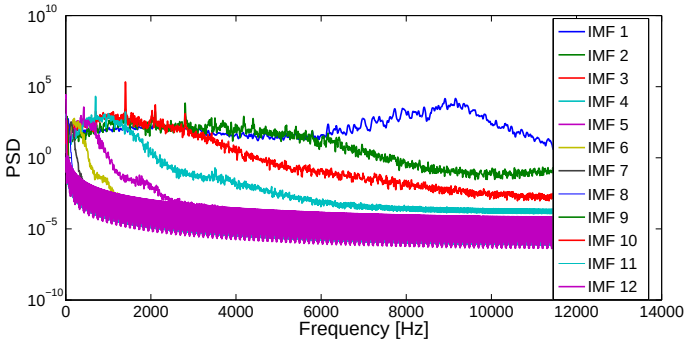

(b) Dataset 11/2/2010.

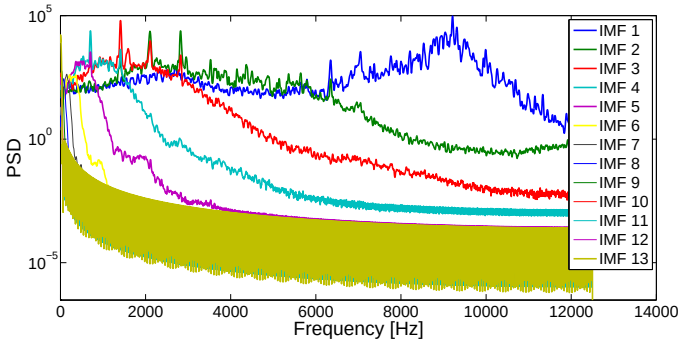

(c) Dataset 4/4/2010.

Figure 28: PSD of the decomposed IMFs for each dataset.

two datasets (11/2/2010) and (4/4/2010). The proposed method therefore might have a potential use in cases were both load and speed vary.

6. Discussion and conclusion

This study has two main purposes. The first one is to test a recently emerged amplitude-frequency separation technique in order to perform time-frequency analysis based condition monitoring with the use of the EMD

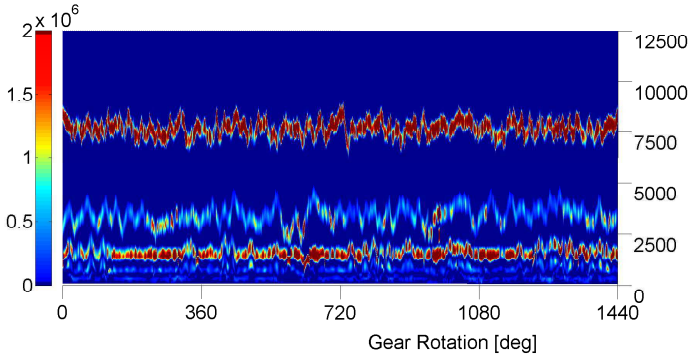

(a) The Teager spectrum of dataset 31/10/2009.

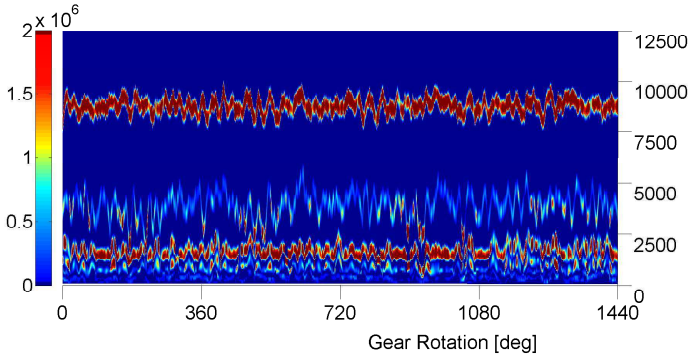

(b) The Teager spectrum of dataset 11/2/2010.

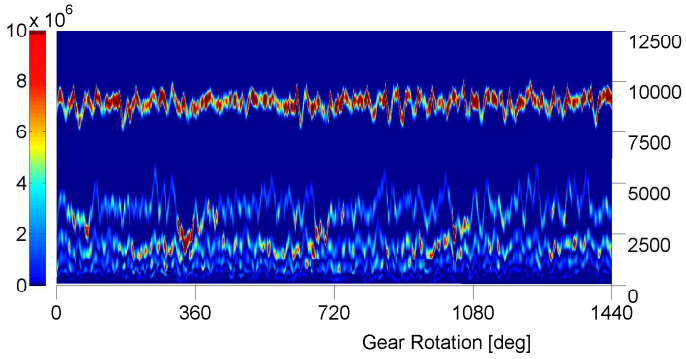

(c) The Teager spectrum of dataset 4/4/2010.

Figure 29: The Teager Spectra of the three datasets. The horizontal axis shows the approximate gear rotation and the vertical axis the instantaneous frequency.

method. The second one is to examine the effect of time-varying load conditions present in wind turbine gearboxes when trying to perform condition monitoring of such systems. Concerning the first aim of the work, it was shown that the TKEO, in combination with the Desa-1 energy separation

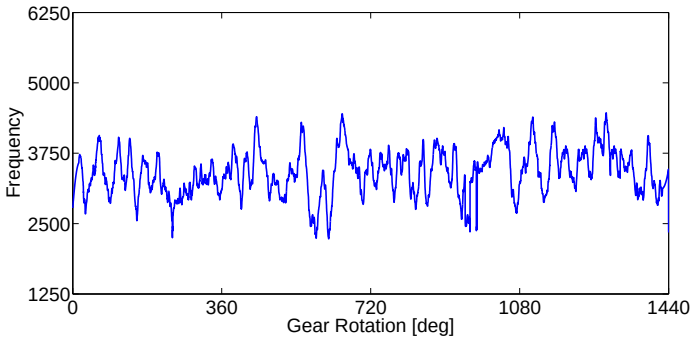

(a) Dataset 31/10/2009.

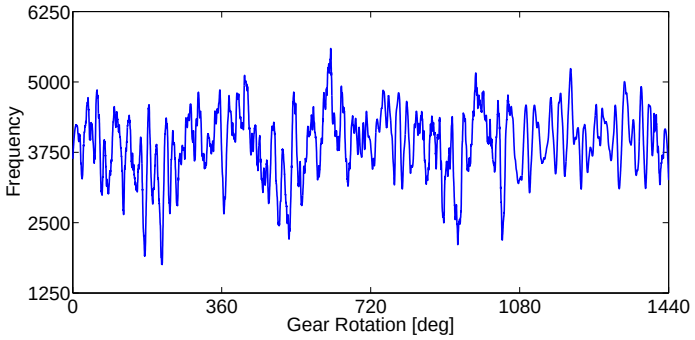

(b) Dataset 11/2/2010.

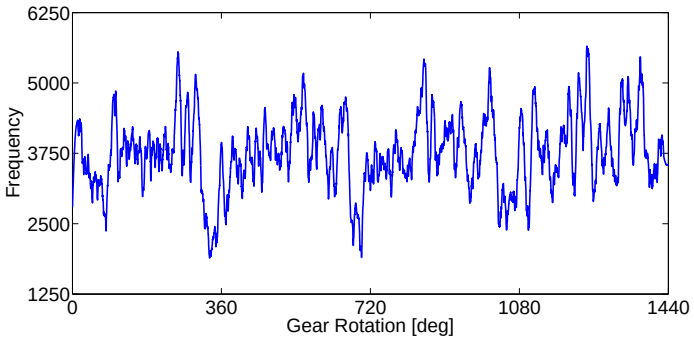

(c) Dataset 4/4/2010.

Figure 30: Instantaneous frequency diagrams (TKEO/ Desa-1) of the 2nd IMF.

algorithm, can be a good alternative approach to the HT, since it offers, under the condition of analysing monocomponent, smooth and clean signals, at least the same quality results as the HT. Concerning the second aim of the study, both the results of a simulated nonlinear gear model that included varying load conditions similar to those produced in wind turbines, as well as the results of real wind turbine gearbox data, confirmed that varying loads can create difficulties in condition monitoring. The EMD

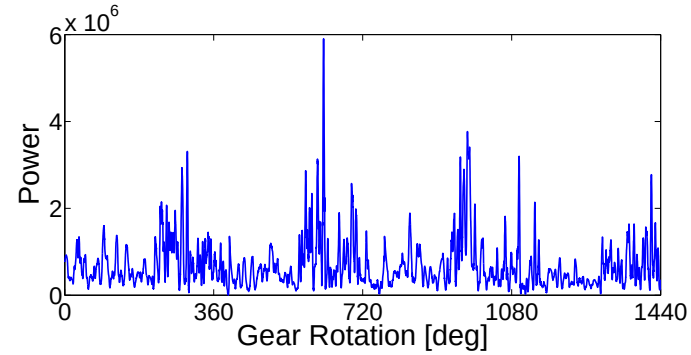

(a) Dataset 31/10/2009.

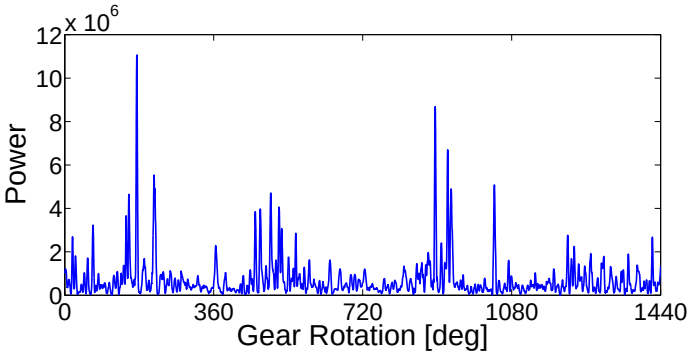

(b) Dataset 11/2/2010.

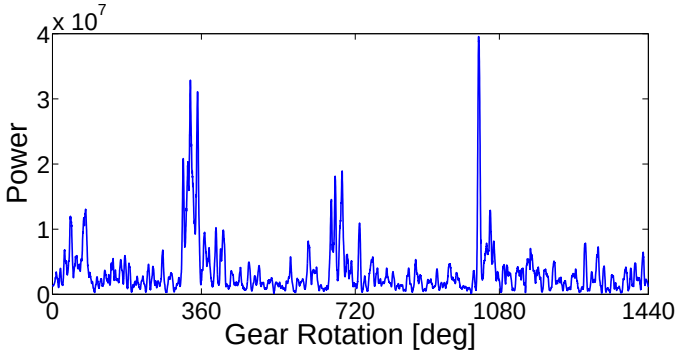

(c) Dataset 4/4/2010.

Figure 31: Power (TKEO/ Desa-1) of the 2nd IMF.

method managed to separate the major part of the time-varying load influences from the vibration signals, leaving signal components that could be related to damage, available for further analysis either with the HT or the TKEO techniques. The time-frequency analysis performed with the TKEO approach successfully extracted damage sensitive features. More particularly the instantaneous amplitude, or an estimated measure of power, of the IMF that corresponds to the frequency region of the harmonics of the

meshing frequency of the damaged gear pair can indicate the existence of damage as periodic pulses. The instantaneous frequency can be also used for the extraction of features, since frequency drops appear at the same IMF. A hypothesis, initially made due to the results of the simulations, and which suggested that the number of IMFs might be an indication of damage and/or different load conditions in the datasets examined (with certain restrictions), was not confirmed or contradicted by the experimental datasets analysed in this study. Therefore, further research might be of interest on this subject.

7. Acknowledgements

This work is part of the SYSWIND project, under the Marie Curie Network, and funded by the European Commission Seventh Framework Program. The support of the UK Engineering and Physical Sciences Research Council (EPSRC) through grant reference no. EP/J016942/1 is also greatly acknowledged.

The authors would also like to thank the reviewers for their insightful comments that helped significantly in improving this paper.

8. References

[1] Wind turbine data summary table 2. WindStats Newsletter 2007;1:20.

[2] Doebling, S.W., Farrar, C.R., Prime, M.B., Shevitz, D.W.. Damage identification and health monitoring of structural and mechanical systems from changes in their vibration characteristics: A literature review. Los Alamos National Laboratory 1996;.

[3] Antoni, J.. The spectral kurtosis: a useful tool for characterising non-stationary signals. Mechanical Systems and Signal Processing 2006;20:282–307.

[4] Inalpolat, M., Kahraman, A.. A theoretical and experimental investigation of modulation sidebands of planetary gear sets. Journal of Sound and Vibration 2009;323(3-5):677–696.

[5] Inalpolat, M., Kahraman, A.. A dynamic model to predict modulation sidebands of a planetary gear set having manufacturing errors. Journal of Sound and Vibration 2010;329(4):371–393.

[6] Badaoui, M.E., Guillet, F., Danière, J.. New applications of the real cepstrum to gear signals, including definition of a robust fault indicator. Mechanical Systems and Signal Processing 2004;18(5):1031–1046.

[7] Staszewski, W.J., Worden, K., Tomlinson, G.R.. Time-frequency analysis in gearbox fault detection using the wigner-ville distribution and pattern recognition. Mechanical Systems and Signal Processing 1997;11(5):673–692.

[8] Staszewski, W.J., Tomlinson, G.R.. Application of the wavelet transform to fault detection in a spur gear. Mechanical Systems and Signal Processing 1994;8(3):289–307.

[9] Antoni, J., Randall, R.B.. Differential diagnosis of gear and bearing faults. Journal of Vibration and Acoustics 2009;124(2):165–171.

[10] Peng, Z.K., Chu, F.L.. Application of the wavelet transform in machine condition monitoring and fault diagnostics: a review with bibliography. Mechanical Systems and Signal Processing 2004;18(2):199–221.

[11] Huang, N.E., Shen, Z., Long, S.R., Wu, M.C., Shih, H.H., Zheng, Q., et al. The empirical mode decomposition and the hilbert spectrum for nonlinear and non-stationary time series analysis. Proceedings of the Royal Society of London Series A: Mathematical, Physical and Engineering Sciences 1998;454(1971):903–995.

[12] Ricci, R., Pennacchi, P.. Diagnostics of gear faults based on emd and automatic selection of intrinsic mode functions. Mechanical Systems and Signal Processing 2011;25(3):821 – 838.

[13] Parey, A., Badaoui, M.E., Guillet, F., Tandon, N.. Dynamic modelling of spur gear pair and application of empirical mode decomposition-based statistical analysis for early detection of localized tooth defect. Journal of Sound and Vibration 2006;294(3):547 – 561.

[14] Teager, H.M., Teager, S.M.. A phenomenological model for vowel production in the vocal tract. In: Speech Science: Recent Advances; chap. 3. San Diego, CA: College-Hill Press; 1985, p. 73–109.

[15] Teager, H.M., Teager, S.M.. Evidence for nonlinear sound production mechanisms in the vocal tract. In: International Conference on Acoustics, Speech, and Signal Processing; vol. D; chap. 55. France: Kluwer Academic Publications; 1990, p. 241–261.

[16] Kaiser, J.F.. On a simple algorithm to calculate the 'energy' of a signal. In: International Conference on Acoustics, Speech, and Signal Processing; vol. 1. 1990, p. 381–384.

[17] Kaiser, J.F.. On teager's energy algorithm and its generalization to continuous signals. In: Proceedings of IEEE DSP Workshop. New Paltz, NY; 1990,.

[18] Junsheng, C., Dejie, Y., Yu, Y.. The application of energy operator demodulation approach based on emd in machinery fault diagnosis. Mechanical Systems and Signal Processing 2007;21(2):668 – 677.

[19] Antoniadou, I., Manson, G., Dervilis, N., Taylor, S.G., Worden, K., Farrar, C.R.. Damage detection of raptor telescope systems using time-frequency analysis methods. In: 5th International Congress on Technical Diagnostics. September 2012,.

[20] Feng, Z., Liang, M., Zhang, Y., Hou, S.. Fault diagnosis for wind turbine planetary gearboxes via demodulation analysis based on ensemble empirical mode decomposition and energy separation. Renewable Energy 2012;47(0):112 – 126.

[21] Bartelmus, W., Chaari, F., Zimroz, R., Haddar, M.. Modelling of gearbox dynamics under time-varying nonstationary load for distributed fault detection and diagnosis. European Journal of Mechanics - A/Solids 2010;29(4):637 – 646.

[22] Bartelmus, W., Zimroz, R.. Vibration condition monitoring of planetary gearbox under varying external load. Mechanical Systems and Signal Processing 2009;23(1):246 – 257.

[23] Stander, C., Heyns, P.. Instantaneous angular speed monitoring of gearboxes under non-cyclic stationary load conditions. Mechanical Systems and Signal Processing 2005;19(4):817 – 835.

[24] Stander, C., Heyns, P., Schoombie, W.. Using vibration monitoring for local fault detection on gears operating under fluctuating load conditions. Mechanical Systems and Signal Processing 2002;16(6):1005 – 1024.

[25] Kahraman, A., Singh, R.. Non-linear dynamics of a spur gear pair. Journal of Sound and Vibration 1990;142(1):49–75.

[26] Kahraman, A., Singh, R.. Non-linear dynamics of a geared rotor-bearing system with multiple clearances. Journal of Sound and Vibration 1991;144(3):469–506.

[27] Kahraman, A., Singh, R.. Interactions between time-varying mesh stiffness and clearance non-linearities in a geared system. Journal of Sound and Vibration 1991;146(1):135–156.

[28] Parker, R., Vijayakar, S., Imajo, T.. Non-linear dynamic response of a spur gear pair: Modelling and experimental comparisons. Journal of Sound and Vibration 2000;237(3):435–455.

[29] Theodossiades, S., Natsiavas, S.. Non-linear dynamics of gear-pair systems with periodic stiffness and backlash. Journal of Sound and Vibration 2000;229(2):287–310.

[30] Theodossiades, S., Natsiavas, S.. Periodic and chaotic dynamics of motor-driven gear-pair systems with backlash. Chaos, Solitons & Fractals 2001;12(13):2427–2440.

[31] Vaishya, M., Singh, R.. Analysis of periodically varying gear mesh systems with coulomb friction using floquet theory. Journal of Sound and Vibration 2001;243(3):525–545.

[32] Lim, T., Singh, R.. Vibration transmission through rolling element bearings. part iii: Geared rotor system studies. Journal of Sound and Vibration 1991;151(1):31–54.

[33] Ozguven, H.N., Houser, D.. Mathematical models used in gear dynamicsa review. Journal of Sound and Vibration 1988;121(3):383–411.

[34] Wang, J., Li, R., Peng, X.. Survey of nonlinear vibration of gear transmission systems. Applied Mechanics Reviews 2003;56(3):309–329.

[35] Parey, A., Tandon, N.. Spur gear dynamic models including defects: A review. The Shock and Vibration Digest 2003;35:465–478.

[36] Jonkman, J.. Aerodyn, fast and adams design codes 2012;URL `http://wind.nrel.gov/designcodes/simulators`.

[37] Smith, J.D.. Gear noise and vibration 1999;.

[38] Endo, H., Randall, R.B., Gosselin, C.. Differential diagnosis of spall vs. cracks in the gear tooth fillet region: Experimental validation. Mechanical Systems and Signal Processing 2009;23(3):636–651.

[39] Howard, I., Jia, S., Wang, J.. The dynamic modelling of a spur gear in mesh including friction and a crack. Mechanical Systems and Signal Processing 2001;15(5):831 – 853.

[40] Chaari, F., Baccar, W., Abbes, M.S., Haddar, M.. Effect of spalling or tooth breakage on gearmesh stiffness and dynamic response of a one-stage spur gear transmission. European Journal of Mechanics - A/Solids 2008;27(4):691–705.

[41] Feldman, M.. In: Hilbert transform applications in mechanical vibration. Wiley; 2011,.

[42] Flandrin, P., Rilling, G., Goncalves, P.. Empirical mode decomposition as a filter bank. Signal Processing Letters, IEEE 2004;11(2):112 – 114.

[43] Wu, Z., Huang, N.E.. Ensemble empirical mode decomposition: A noise-assisted data analysis method. Advances in Adaptive Data Analysis 2009;1:1 – 49.

[44] Gledhill, R.J.. Methods for investigating conformational change in biomolecular simulations. PhD Thesis, University of Southampton 2003;:201.

[45] Hilbert, D.. Grundzüge einer allgemeinen, therie der linearen integralgleichungen 1953;.

[46] Gabor, D.. Theory of communication. Journal Institution of Electrical Engineers London 1946;93(3):429–457.

[47] Maragos, P., Kaiser, J.F., Quatieri, T.F.. Energy separation in signal modulations with application to speech analysis. IEEE Transactions on Signal Processing 1993;41(10):3024–3051.

[48] Kvedalen, E.. Signal processing using the teager energy operator and other nonlinear operators. PhD Dissertation 2003;.

[49] Worden, K., Tomlinson, G.. Nonlinearity in structural dynamics: Detection, identification and modelling. Institute of Physics Publishing 2001;.